Eng. Sci., 2025, **36**, 1672

Engineered Science
DOI: https://dx.doi.org/10.30919/es1672

Dynamics of a Vertical Unbalanced Gas Centrifuge Supported by Magnetic Bearings

Almatbek Kydyrbekuly,[1] Gulama-Garip Alisher E. Ibrayev,[1,*] Rakhmetolla A.Sh.[1] and Shabdan E.[2]

Abstract

The gas centrifuge is modeled as a rigid rotor supported by two magnetic bearings with eight-pole structures. To describe the system dynamics, the coupled nonlinear ordinary differential equations (ODE) of the second order are derived, to solve which the Fourier method (FM) is used, *i.e.* the solution to the system of differential equations of motion is obtained in the form of a trigonometric series. The use of FM provides the possibility of representing a harmonic semi-analytical solution. The dynamics of forced vibrations and self-excited vibrations under the action of harmonic forces is studied, and free oscillations are analyzed. Various parameters influencing the vibration behavior of the rotor are studied. The dependence of the amplitudes and phases of vibrations on the excitation frequency is analysed. Ultraharmonic and subharmonic vibrations, as well as self-excited vibrations of the gas centrifuge on magnetic bearings (GCMB or a rotor) are studied.

Keywords: Gas centrifuge; Magnetic bearings; Nonlinear vibrations; Rotor system.
Received: 13 June 2025; Revised: 13 July 2025; Accepted: 01 August 2025
Article type: Original research.

1. Introduction

Magnetic bearings (MB) are one of the most innovative developments in turbomachinery and, therefore, they are widely used in various rotary machines[1–2] including turbo compressors, turboexpanders, generators, turbines, pumps,[3–4] electric motors, gas centrifuges, machine tools,[5] as well as in medical devices, robotics, space equipment, contactless drives, vibration isolation and flywheel energy storage devices. For numerical study of rotor dynamics in magnetic bearings, specialists use mathematical models, similar to the corresponding models of rotors in elastic supports, but taking into account the specific features manifested in the interaction of magnetic, electromagnetic and electric fields, and the forces caused by this interaction. A rotor system with a magnetic bearing is a nonlinear system as all components in the structure of the magnetic bearings of various types, namely, permanent magnets or electromagnets, power amplifiers, controllers and even position sensors are characterized by nonlinear dependencies of various parameters. A mathematical description of the dynamic behavior of a rotor in magnetic bearings makes it possible to adequately reflect the nonlinear relationship of electrical, magnetic and mechanical processes in such a system, and will also allow a more accurate recording and analysis of the equations of system vibrations.[6] Recently, a large number of works have been devoted to the study of dynamics of rotors in magnetic bearings, where nonlinear forces of influence are considered.[7–38] An analysis of models with one or two degrees of freedom, which are usually used to describe the dynamics of rotors in magnetic bearings, makes it possible to trace the qualitative characteristics of the system and conduct fundamental research. Mohamed and Emad[7] investigated nonlinear vibrations of a rigid rotor in a magnetic field taking into account the gyroscopic moment and showed that Hopf bifurcations and instability of periodic motion can be present in the system. Laier[8] showed the possibility of transitions from one stable branch of the resonance curve to another using numerical integration of a system of differential equations. Springer[9] modeled non-stationary nonlinear vibrations of a rotor taking into account the nonlinearity of the magnetic force and the saturation of the core material of radial magnetic fields. Steinschaden *et al.*[10] studied the influence of nonlinear forces on active magnetic rotors and their periodic responses using numerical integration. Ji *et al.*[11] presented the magnetic force as a Taylor series expansion with preservation of the third-order nonlinear terms. Using the normal form method, they showed that the system can exhibit saddle-node

[1]*Al-Farabi Kazakh National University, Almaty, 050038, Kazakhstan*
[2]*Astana IT University, Astana, Akmola Region, 010000, Kazakhstan*
[*]*Email:* ybraev.alysher@mail.ru (G. Ibrayev)

bifurcations and Hopf bifurcations. They also investigated a periodically forced system with one degree of freedom with feedback and saturation constraint. It was shown[12] that the nonlinearities taken into account can lead to the appearance of an asymmetric, subharmonic and chaotic response. For this mathematical model, Ji and Hansen proposed a method of analysis using the asymptotic method. The approximate solutions obtained using this method were in close agreement with the reference results of numerical integration. To analyze the dynamic behavior the authors[13–14] used the Lyapunov exponents, bifurcation diagrams, phase portraits, basins of attraction and Poincaré maps. To analyze the same mathematical model they used two methods to approximate the super harmonic resonant response of a piecewise nonlinear oscillator: the modified averaging method and the matching method. Both methods[15] are in good agreement with direct numerical simulation, but the matching method is more accurate. Virgin *et al.*,[16] studying the nonlinear dynamics of a rotor with two degrees of freedom, showed the influence of the geometric relationship between two pairs of electromagnet poles creating forces in mutually perpendicular directions.

Chinta *et al.* investigated the nonlinear periodic responses of a rotor with geometrically coupled magnetic bearings using the trigonometric collocation method and numerical integration. They showed the occurrence of a cyclic bifurcation, which leads to a stepwise change in frequency.[17] Ji *et al.* investigated the motion of a rotor with active magnetic bearings under fundamental resonance conditions, taking into account the nonlinear dependence of the force, current and displacement in the electromagnets. Using the multiscale method to reduce the system to four averaged equations, they showed the presence of saddle-node bifurcations and Hopf bifurcations in the system.[18–19] A study of the same rotor-magnetic bearing system under super harmonic motions shows the possibility of stability loss.[20] In systems with magnetic bearings, the equilibrium can become unstable due to Hopf bifurcations both without external excitation effects and under the action of loads on the rotor caused by the imbalance.[21–22] Ho and Liu showed that the influence of a thrust active magnetic bearing on radial vibrations can lead to a decrease in the limiting stability speed and the occurrence of Hopf bifurcations during processional motion along the first form of transverse oscillations.[23] Zhang *et al.* studied the nonlinear dynamics of a rotor on active magnetic bearings taking into account the periodically changing stiffness caused by the operation of a PD controller. The application of the asymptotic perturbation method shows the possibility of the occurrence of periodic, quasi-periodic and chaotic vibrations with modulated amplitude.[24] It is shown that in a system with periodically changing rigidity and nonlinear electromagnetic force, jumps from one mode to another are possible.[25] Inayat-Hussain considered a rigid rotor on active magnetic bearings taking into account the nonlinear dependence of electromagnetic forces, current and air gap. He showed the possibility of nonlinear phenomena appearing in the system, such as duality of stable modes, breakdowns and jumps of amplitudes, synchronous, subsynchronous, quasi-periodic and chaotic oscillations.[26] Heydari *et al.* showed that the homotopy perturbation method has the second order of accuracy in the context of studying a rotor on two eight-pole active magnetic bearings (hereinafter MB), and the system itself is stably maintained due to the MB.[27] To study stability of a rotor on 16-pole magnetic bearings, Zhang *et al.* applied the asymptotic perturbation method.[28] The multiple scales method is widely used to analyze the stability and dynamics of rotor systems, including systems with magnetic bearings.[29–33] Shaw *et al.* presented an algorithm for applying the normal forms dimensionality reduction method to rotor systems.[34] This method was also applied by Ji in his work to determine the direction and stability of Hopf bifurcations.[35] Yektanezhad applied the renormalization group method directly to the equations describing a flexible rotor on a magnetic bearing to analyze the fundamental resonance.[36] The harmonic balance method is also often used to analyze the resonant modes of rotors on magnetic bearings.[37,38] Saeed *et al.* investigate the nonlinear dynamics of a rotor–active magnetic bearing (AMB) system, taking into account the effects of contact and friction between the rotor and the stator poles. When contact occurs, the system exhibits the possibility of periodic, quasi-periodic, and chaotic oscillations.[39] Li considers a method for dynamic balancing of a rotor supported by magnetic bearings. In this approach, rotor position and bearing current signals are utilized in active vibration control to identify the residual unbalance.[40] S. M. El-Shourbagy *et al.* conducted a stability analysis, determined stability boundaries, and demonstrated the emergence of bifurcations in a rotor system equipped with a 12-pole magnetic bearing. Such a configuration was shown to possess improved stability under vibratory conditions.[41] Trentini examines a dynamic model of an eight-pole magnetic bearing, represented by equations of motion that incorporate gyroscopic and magnetic forces. The model also accounts for the influence of pole area, bias current, and air gap.[42] To reduce vibrations in rotor–AMB systems, Zhang *et al.* employed a base acceleration feedforward compensation algorithm. Experimental implementation of this algorithm significantly reduced rotor vibrations under both harmonic and random base excitations.[43] To further suppress rotor vibrations in active magnetic bearing systems, a controller is proposed that enables a smoother control signal.[44] In the case of eight-pole magnetic bearings, the influence of pole arrangement on rotor vibrations is studied. The model is based on linear displacement theory and assumes that the rotor undergoes transverse oscillations.[45] Ma *et al.* investigate a rotor–AMB system model with 12 poles and variable stiffness. The dynamic behavior is analyzed using averaged equations of motion derived via the method of multiple scales, considering primary parametric and subharmonic resonances. Numerical simulations are carried out using MATLAB. It is shown that depending on the amplitude of the parametric excitation, the system may exhibit period-one, period-two, and chaotic

oscillations.[46] In contrast to the aforementioned studies, the present work provides a comprehensive investigation of the motion of a rotor system supported by magnetic bearings, considering forced, ultraharmonic, and subharmonic oscillations, as well as self-excited vibrations. The conditions under which the rotor performs precessional motion are determined. In addition, the conditions under which the centrifuge exhibits circular and elliptical precessional motions are identified. Using the describing function method, the amplitudes and frequencies of the system's oscillations are determined in cases where subharmonic and ultraharmonic components are superimposed on the forced vibrations.

2. Materials and methods

2.1 Problem statement and equations of motion

The rotor system is a vertical hollow unbalanced cylinder, the length of which is much greater than its width, supported by two active magnetic bearings with eight pole structures. The basic equations of the system dynamics are derived as two coupled nonlinear ordinary differential equations of the second order. The proportional-differential (PD) controllers are used to control the rotor movements that cause imbalance in the system. A model of the rotor system is shown in Fig. 1.

The stator has eight pairs of poles. For simplicity, saturation and hysteresis of the magnetic core material, eddy

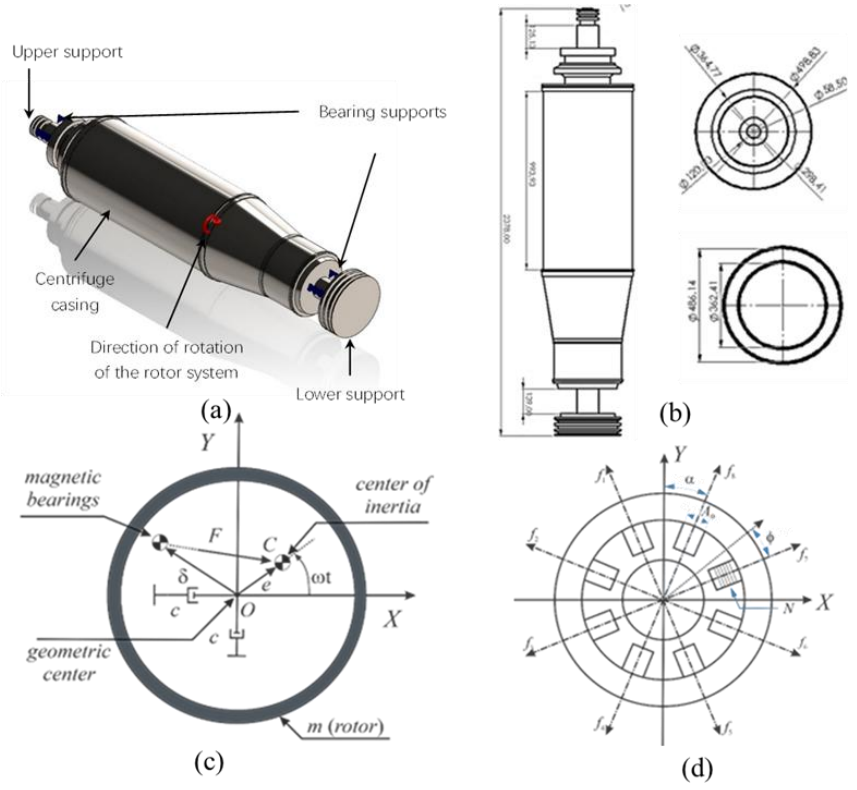

Fig. 1: a) Vertical rotor system on magnetic bearings. b) Dimensions of the prototype installation. c) Dynamic model of the rotor system. d) Electromagnetic forces directed from the bearing to the rotor.

current losses and all other secondary factors are neglected here. It is assumed that all magnets have the same design and the same number of windings. According to the theory of electromagnetism, the electromagnetic force f_i generated by each pair of electromagnets, can be expressed as follows:[6]

$$f_i = -\frac{\mu_0 A_0 N^2 I_i^2 \cos\varphi}{4\delta_i^2}, \left(i = \overline{1,8}\right) \quad (1)$$

Here μ_0 is permeability (a magnetic constant); N is the number of turns around the core; A_0 is the effective cross-sectional area of one electromagnet; δ_i is the distance between the bearing and rotor cores when the rotor is displaced from the equilibrium position; I_i is the current in the coils. It is seen that the force varies non-linearly with the coil current and the distance between the bearing and rotor cores. When the rotor deviates from the center of the bearings, the radial clearance is expressed as

$$\begin{aligned} \delta_i &= c_0 \pm x\sin\alpha \mp y\cos\alpha, i = 1,5 \\ \delta_i &= c_0 \pm x\sin\alpha \pm y\cos\alpha, i = 4,8 \\ \delta_i &= c_0 \pm x\sin\alpha \mp y\cos\alpha, i = 2,6 \\ \delta_i &= c_0 \pm x\sin\alpha \pm y\cos\alpha, i = 3,7 \end{aligned} \quad (2)$$

where c_0 is the steady-state air gap, α is the angle defined in Fig. 1, and x,y is the rotor offset from the bearing center. For magnetically suspended rotors, various control methods have been used to achieve different goals. Here, only the PD controller is considered:[6]

$$\begin{aligned} i_x &= k_p x + k_d \dot{x}, \\ i_x &= k_p y + k_d \dot{y}, \end{aligned} \quad (3)$$

where k_p is a proportional gain coefficient; k_d is the constant of the derivative control. The coil current is determined by the formulas

$$\begin{aligned} I_1 &= I_8 = I_0 - i_y \\ I_4 &= I_5 = I_0 + i_y \\ I_6 &= I_7 = I_0 - i_x \\ I_2 &= I_3 = I_0 + i_x \end{aligned} \tag{4}$$

where I_0 is the pre-magnetization current. The pre-magnetization current is used to reduce the nonlinearity of the magnetic force and the currents arising near the equilibrium state. The total electromagnetic forces in the directions of the *Ox* and *Oy* axes are expressed as

$$\begin{aligned} F_x &= (f_6 + f_7 - f_2 - f_3)\cos\alpha \\ &\quad + (f_5 + f_8 - f_1 - f_4)\sin\alpha, \\ F_y &= (f_1 + f_8 - f_4 - f_5)\cos\alpha \\ &\quad + (f_2 + f_7 - f_3 - f_6)\sin\alpha. \end{aligned} \tag{5}$$

Then the equations of motion of an unbalanced rotor (GCMB) will be written as

$$\begin{aligned} m\ddot{x} + c\dot{x} &= F_x + me\omega^2\cos\omega t, \\ m\ddot{y} + c\dot{y} &= F_y + me\omega^2\sin\omega t, \end{aligned} \tag{6}$$

where m is the mass, e is the eccentricity, ω is the angular velocity of the rotor; c is the damping coefficient. Substituting Eq. (2)-(4) into Eq. (1), we obtain the force as a nonlinear function of the control current and the distance between the rotor and the bearing in the x and y directions. The force f_i is expanded in a Taylor series in the vicinity of the point $x = y = 0$, and then the higher-order nonlinear terms are omitted. As a result, we obtain the equations of motion of an unbalanced rotor (GCMB) in the form

$$\begin{aligned} &\ddot{x} + 2h\dot{x} + \omega_0^2 x - k_1x^3 - k_2xy^2 - k_3\dot{x}x^2 - \\ &k_4\dot{x}y^2 - k_5x\dot{y}^2 - k_6x\dot{x}^2 - k_7xy\dot{y} = \\ &2f\cos\omega t, \\ &\ddot{y} + 2h\dot{y} + \omega_0^2 y - k_1y^3 - k_2yx^2 - k_3\dot{y}y^2 - \\ &k_4\dot{y}x^2 - k_5y\dot{x}^2 - k_6y\dot{y}^2 - k_7xy\dot{x} = \\ &2f\sin\omega t. \end{aligned} \tag{7}$$

Here

$$\begin{aligned} F_x &= me\omega^2(-\omega_0^2 x + k_1x^3 + k_2xy^2 + k_3\dot{x}x^2 + \\ &k_4\dot{x}y^2 + k_5x\dot{y}^2 + k_6x\dot{x}^2 + k_7xy\dot{y}), \\ F_y &= me\omega^2(-\omega_0^2 y + k_1y^3 + k_2yx^2 + k_3\dot{y}y^2 + \\ &k_4\dot{y}x^2 + k_5y\dot{x}^2 + k_6y\dot{y}^2 + k_7xy\dot{x}) \end{aligned} \tag{8}$$

are the components of electromagnetic forces.
The coefficients of Eq. (7) and (8) are written as

$$\begin{aligned} &2h = 8d\cos\alpha + c_1, \Omega^2 = 8(p\cos\alpha - 1), \\ &k_1 = 16(\cos^4\alpha + \sin^4\alpha) - 24p\cos^3\alpha + \\ &8p^2\cos^2\alpha, \\ &k_2 = 96\cos^2\alpha\sin^2\alpha - 72p\cos\alpha\sin^2\alpha + \\ &8p^2\sin^2\alpha, \\ &k_3 = -8d\cos^2\alpha(3\cos\alpha - 2p), \\ &k_4 = -24d\cos\alpha\sin^2\alpha, \\ &k_5 = 8d^2\sin^2\alpha, \\ &k_6 = 8d^2\cos^2\alpha, \\ &k_7 = 16pd\sin^2\alpha - 48d\sin^2\alpha\cos\alpha. \end{aligned} \tag{9}$$

where

$$\begin{aligned} &p = \frac{k_p c_0}{I_0}, d = \frac{k_d c_0}{I_0 B^2}, B^2 = \frac{4mc_0^3}{\mu_0 N^2 A_0 I_0^2}, c_1 = \frac{cc_0}{B}, c_2 = \\ &e\omega^2 I_0, 2f = \frac{B^2 c_2}{\cos\alpha}, \end{aligned}$$

p – stiffness coefficient of the system, d – damping coefficient, c_1 – damping parameter, f – dimensionless eccentricity, B is a dimensionless parameter of the time variable.

2.2 Solution of the equations of motion

2.2.1 Free vibrations

Let us consider free vibrations of the rotor, *i.e.* the case when there is no disturbing force. We will assume that the rotor without imbalance performs free vibrations with the frequency Ω and amplitude a. Then the solution of the system of Eq. (7) is written as

$$\begin{aligned} x &= a\cos\Omega t \\ y &= a\sin\Omega t \end{aligned} \tag{10}$$

On the complex plane this solution has the form

$$z = x + iy = ae^{i\Omega t}. \tag{11}$$

Substituting Eq. (11) into system (7), and including the phase angle φ in the expression for the disturbing force and then equating the coefficients of the functions $\cos\Omega t$ and $\sin\Omega t$, we get

$$\begin{aligned} &4(\omega_0^2 - \Omega^2) = a^2[3k_1 + k_2 + \Omega^2(3k_5 + k_6)] \\ &a^2(k_3 + 3k_4 - k_7) = 2h \end{aligned} \tag{12}$$

From system (12) we determine the amplitude a and frequency Ω of free vibrations of the rotor

$$\begin{aligned} &a = \sqrt{((4(\omega\_0\hat{}2 - \Omega\_\hat{}2))/([e\_2 + \\ &\Omega\_\hat{}2\ e\_3)]),)\ \Omega = \sqrt{((4\omega\_0\hat{}2 - e\_2\ e\_4)/} \\ &(4 + e\_3\ e\_4\ )). \end{aligned} \tag{13}$$

were

$$\begin{aligned} &e_0 = 4(\omega_0^2 - \Omega^2), e_1 = (k_3 + 3\,k_4 - k_7), e_2 = 3k_1 + \\ &k_2, e_3 = 3k_5 + k_6, e_4 = \frac{2h}{e_1}. \end{aligned}$$

Let us consider the general case of free vibrations of the rotor, *i.e.*, when its axis moves along an ellipse. In this case, the system of Eq. (7) will take the form

$$\begin{aligned} &4(\omega_0^2 - \Omega^2) - (3k_1 + \Omega^2 k_6)a^2 - (k_2 + \\ &3\Omega^2 k_5)b^2 = 0 \\ &k_3a^2 + (3k_4 - k_7)b^2 = 8h \\ &4(\omega_0^2 - \Omega^2) - (3k_1 + \Omega^2 k_6)b^2 - (k_2 + \\ &3\Omega^2 k_5)a^2 = 0 \\ &k_3b^2 + (3k_4 - k_7)a^2 = 8h \end{aligned} \tag{14}$$

Hence

$$a = \sqrt{\eta_0 - \frac{\eta_1(d_1\eta_0 - e_0)}{d_1\eta_1 - d_2}}, b = \sqrt{\frac{d_1\eta_0 - e_0}{d_1\eta_1 - d_2}} \tag{15}$$

where

$\eta_0 = \frac{8h}{k_3}, \eta_1 = \frac{3k_4 - k_7}{k_3}, e_0 = 4(\omega_0^2 - \Omega^2), d_1 = (3k_1 + \Omega^2 k_6), d_2 = (k_2 + 3\Omega^2 k_5)$.

2.2.2 Forced vibrations

To solve the problem of vibrations of the GCMB, we use the harmonic balance method. Let us consider the simplest case, *i.e.* when the shaft center makes a circular precession motion around the equilibrium position. We find the conditions under which such a motion of the GCMB can exist. In this case, we will represent the solution of the system of Eq. (7) in the form

$$\begin{aligned} x &= a\cos\omega t, \\ y &= a\sin\omega t. \end{aligned} \tag{16}$$

On the complex plane this solution is written as

$$z = x + iy = ae^{i\omega t}. \tag{17}$$

Substituting Eq. (16) into system (7), including the phase angle φ in the expression for the disturbing force and equating the coefficients of the functions $\cos\omega t$ and $\sin\omega t$ we get

$$\begin{aligned} &a\left(\omega_0^2 - \omega^2 - \frac{a^2}{4}(3k_1 + k_2 + \omega^2(3k_5 + k_6))\right) = 2f\cos\varphi, \omega a\left(\frac{a^2}{4}(k_3 + 3k_4 - k_7) - 2h\right) = 2f\sin\varphi. \end{aligned} \tag{18}$$

From system (18) we find an algebraic equation of the 6-th degree with respect to a. By denoting $a^2 = v$ and substituting $u = v + \frac{r}{3}$ we obtain a cubic equation, from which the square of the amplitude of forced vibrations of the rotor a and the expression for the phase angle of displacement φ are determined.

$$u^3 + p_0 u + q_0 = 0, \tag{19}$$

where

$p_0 = \frac{3s - r^2}{3}, q_0 = \frac{2r^3}{27} - \frac{rs}{3} + t, r = -2\frac{e_0 d_0 + d_1 d_2}{d_0^2 + d_1^2}, s = \frac{e_0^2 + d_2^2}{d_0^2 + d_1^2}, t = -\frac{d_3}{d_0^2 + d_1^2},$
$e_0 = 4(\omega_0^2 - \omega^2), d_0 = 3k_1 + k_2 + \omega^2(3k_5 + k_6), d_1 = \omega(k_3 + 3k_4 - k_7), d_2 = 8h\omega, d_3 = 8f.$

The roots of Eq. (19) are determined by Cardano's formulas

$$u_1 = \xi + \zeta, u_2 = \varepsilon_1\xi + \varepsilon_2\zeta, u_3 = \varepsilon_2\xi + \varepsilon_1\zeta, \tag{20}$$

where

$\xi = \left(-\frac{q_1}{2} + \sqrt{D}\right)^{\frac{1}{3}}, \zeta = \left(-\frac{q_1}{2} - \sqrt{D}\right)^{\frac{1}{3}}, D = \left(\frac{p_1}{3}\right)^3 + \left(\frac{q_1}{2}\right)^2, \varepsilon_{1,2} = \frac{-1 \pm i\sqrt{3}}{2}.$

Smoothly changing the rotor speed ω over a wide range at various fixed values of the rotor parameters (GCMB) and magnetic bearings, we find the amplitudes of forced vibrations of the rotor a. Based on these values, we can plot the curves of the amplitude-frequency and phase-frequency responses (hereinafter AFR and PFR) in the plane (ω, a). They are shown in Figs. 3-7.

Let us consider the general case, when the rotor performs a synchronous precession with a frequency ω and its axis of rotation moves along an ellipse, that is:

$$\begin{aligned} x &= a\cos\omega t \\ y &= b\sin\omega t \end{aligned} \tag{21}$$

Substituting (19) into (8) we obtain expressions for the components of electromagnetic forces

$$\begin{aligned} F_x &= ma\left(-\omega_0^2 + \frac{1}{4}\left(3k_1a^2 + k_2b^2 + \omega^2(3k_5b^2 + k_6a^2)\right)\right)\cos\omega t - \frac{ma}{4}\omega(k_3a^2 + 3k_4b^2 - k_7b^2)\sin\omega t \\ F_y &= mb\left(-\omega_0^2 + \frac{1}{4}\left(3k_1b^2 + k_2a^2 + \omega^2(3k_5a^2 + k_6b^2)\right)\right)\sin\omega t + \frac{mb}{4}\omega(k_3b^2 + 3k_4a^2 - k_7a^2)\cos\omega t \end{aligned} \tag{22}$$

Now, substituting (21) and (22) into the equations of rotor motion (7) and writing them in the complex form, we obtain

$$\begin{aligned} &a\{4(\omega_0^2 - \omega^2) - [3k_1a^2 + k_2b^2 + \omega^2(3k_5b^2 + k_6a^2)] - i\omega(k_3a^2 + 3k_4b^2 - k_7b^2 - 8h)\}e^{i\omega t} = 8fe^{i\omega t} \\ &b\{-4i(\omega_0^2 - \omega^2) + i[3k_1b^2 + k_2a^2 + \omega^2(3k_5a^2 + k_6b^2)] - \omega(k_3b^2 + 3k_4a^2 - k_7a^2 - 8h)\}e^{i\omega t} = -i8fe^{i\omega t} \end{aligned} \tag{23}$$

From the system of Eq. (23), including the phase angle of displacement φ_1 in the expression of the disturbing force and equating the coefficients of the functions $\cos\omega t$ and $\sin\omega t$, we can find the amplitudes of the forced vibrations of the rotor a and b in the form

$$\begin{aligned} &4(\omega_0^2 - \omega^2)a - [3k_1a^2 + k_2b^2 + \omega^2(3k_5b^2 + k_6a^2)]a = 8f\cos\varphi_1 \\ &\omega a(k_3a^2 + 3k_4b^2 - k_7b^2 - 8h) = 8f\sin\varphi_1 \end{aligned} \tag{24}$$

$$\begin{aligned} &4(\omega_0^2 - \omega^2)b - [3k_1b^2 + k_2a^2 + \omega^2(3k_5a^2 + k_6b^2)]b = 8f\cos\varphi_1 \\ &\omega b(k_3b^2 + 3k_4a^2 - k_7a^2 - 8h) = 8f\sin\varphi_1 \end{aligned} \tag{25}$$

where

$$\varphi_1 = arctg\left(\frac{\omega(k_3a^2 + 3k_4b^2 - k_7b^2 - 8h)}{4(\omega_0^2 - \omega^2) - [3k_1a^2 + k_2b^2 + \omega^2(3k_5b^2 + k_6a^2)]}\right)$$

As the first and second equations of the systems (24) and (25) are equal, we obtain

$$\begin{aligned} &e_0 + [k_2 + 3\omega^2k_5 - (3k_1 + \omega^2k_6)]ab = (3k_1 + \omega^2k_6)(a^2 + b^2) \\ &k_3(a^2 + b^2) + (k_3 - 3k_4 + k_7)ab = 8h \end{aligned} \tag{26}$$

After some mathematical transformations, from system (26) we obtain the following cubic equation

$$\delta^3 + p_1\delta + q_1 = 0 \tag{27}$$

where

$p_1 = \frac{3s_1 - r_1^2}{3}, q_1 = \frac{2r_1^3}{27} - \frac{r_1 s_1}{3} + t_1, \lambda = \delta - \frac{r}{3}, a = \sqrt{\lambda},$
$\mu_5 = \frac{\mu_3}{\mu_4}, \mu_3 = \mu_2 e_0 + 8h\mu_0, \mu_4 = \mu_1\mu_2 + k_3\mu_0, \mu_2 =$
$k_3 - 3k_4 + k_7, \mu_1 = 3k_1 + \omega^2 k_6,$
$\mu_0 = k_2 + 3\omega^2 k_5 - 3k_1 - \omega^2 k_6.$
$r_1 = \frac{\nu_1}{\nu_0}, s_1 = \frac{\nu_2}{\nu_0}, t_1 = -\frac{f_0^2}{\nu_0}, \nu_0 = \mu_0^2 + \mu_7^2, \nu_1 =$
$2(\mu_0\mu_6 + \mu_7\mu_8), \nu_2 = \mu_6^2 + \mu_8^2,$
$f\_0 = 64f\text{^}2, \mu\_6 = e\_0 - \mu\_9\,\mu\_5, \mu\_7 =$
$\omega\mu\_2, \mu\_8 = \omega[(\mu\_5\,(3k\_4 - k\_7) - 8h], \mu\_9 = k\_2 +$
$3\omega\text{^}2\,k\_5.$

The system of Eq. (6) or expressions (7), as well as the system of nonlinear algebraic Eq. (23), has symmetric terms, possesses a certain degree of symmetry and always has a pair of symmetric solutions. Thus, we have determined the values of the amplitude of forced vibrations *a* and *b* (also symmetric to them) in the directions of the *Ox* and *Oy* axes. Smoothly changing the rotor rotation frequency ω over a wide range at various fixed values of parameters of the rotor (GCMB) and magnetic bearings, we find the amplitudes of forced rotor vibrations *a* and *b*. Based on these values, it is possible to construct the curves (AFR) in the planes (ω, *a*), (ω, *b*). The amplitude graphs for synchronous precession when the rotor rotation axis moves along an ellipse with variations in the values of ω_0, *d*, c_1 and *f* are shown in Figs. 8-13.

2.2.3 Super harmonic vibrations

Let us consider the case when the rotor performs forced vibrations under the action of a disturbing force and ultra harmonic vibrations. We will solve this problem using the small parameter method, assuming that the rotor axis displacements from the equilibrium position and their speeds are small quantities. As a matter of fact, they are small quantities. In this regard, the solution to the problem using the small parameter method is quite justified. We suppose that the rotor deviations from the vertical and their speeds are second-order small quantities. Then we will suppose that the rotor displacement from the equilibrium position can be described as

$$\begin{aligned} x &= x_0 + \varepsilon x_1 + \varepsilon^2 x_2 + \cdots \\ y &= y_0 + \varepsilon y_1 + \varepsilon^2 y_2 + \cdots \end{aligned} \tag{28}$$

where ε is a small parameter. In this case, we can write the equations of rotor motion in the form

$$\begin{aligned} &\ddot{x} + 2h\dot{x} + \omega_0^2 x - \varepsilon(k_1 x^3 + k_2 x y^2 + k_3 \dot{x} x^2 + \\ &k_4 \dot{x} y^2 + k_5 x \dot{y}^2 + k_6 x \dot{x}^2 + k_7 x y \dot{y}) = \\ &2fc\cos\omega t \\ &\ddot{y} + 2h\dot{y} + \omega_0^2 y - \varepsilon(k_1 y^3 + k_2 y x^2 + \\ &k_3 \dot{y} y^2 + k_4 \dot{y} x^2 + k_5 y \dot{x}^2 + k_6 y \dot{y}^2 + \\ &k_7 x y \dot{x}) = 2f\sin\omega t \end{aligned} \tag{29}$$

Substituting (57) into (58) and equating the expressions for the same powers of ε, we obtain the equations of the first, second, and higher approximations. Let us write the equations of the first approximation

$$\begin{aligned} \ddot{x}_0 + 2h\dot{x}_0 + \omega_0^2 x_0 &= 2f\cos\omega t \\ \ddot{y}_0 + 2h\dot{y}_0 + \omega_0^2 y_0 &= 2f\sin\omega t \end{aligned} \tag{30}$$

Eq. (59) can be solved using the method of complex amplitudes. For this purpose, we introduce the complex quantity

$$z_0 = x_0 + iy_0 \tag{31}$$

Taking into account (60), Eq. (59) can be written as

$$\ddot{z}_0 + 2h\dot{z} + \omega_0^2 z_0 = 2fe^{i\omega t} \tag{32}$$

Let us use the notation

$$z_0 = A_0 e^{i\omega t} \tag{33}$$

Substituting (33) into (32) we get

$$A_0 = \frac{2f}{\sqrt{(\omega_0^2 - \omega^2)^2 + 4h^2\omega^2}}, \tag{34}$$

$$\varphi_0 = \operatorname{arctg}\left(\frac{2h\omega}{\omega_0^2 - \omega^2}\right) \tag{35}$$

When the amplitude (64) and the phase (65) of vibrations in the first-order approximation are known, then the law of rotor motion has the form

$$\begin{aligned} x_0 &= A_0\cos(\omega t - \varphi_0) \\ y_0 &= A_0\sin(\omega t - \varphi_0) \end{aligned} \tag{36}$$

By equating the expressions at a small parameter ε, we obtain the equations of the second-order approximation

$$\begin{aligned} &\ddot{x}_1 + 2h\dot{x}_1 + \omega_0^2 x_1 = k_1 {x_0}^3 + k_2 x_0 {y_0}^2 + \\ &k_3 \dot{x}_0 {x_0}^2 + k_4 \dot{x}_0 {y_0}^2 + k_5 x_0 {\dot{y}_0}^2 + k_6 x_0 {\dot{x}_0}^2 + \\ &k_7 x_0 y_0 \dot{y}_0 \\ &\ddot{y}_1 + 2h\dot{y}_1 + \omega_0^2 y_1 = k_1 {y_0}^3 + k_2 y_0 {x_0}^2 + \\ &k_3 \dot{y}_0 {y_0}^2 + k_4 \dot{y}_0 {x_0}^2 + k_5 y_0 {\dot{x}_0}^2 + k_6 y_0 {\dot{y}_0}^2 + \\ &k_7 x_0 y_0 \dot{x}_0 \end{aligned} \tag{37}$$

Substituting expressions (36) into the right-hand sides of the equations of system (37) and representing the solution in the form

$$\begin{aligned} x_1 &= A_1\cos(\omega t - \varphi_1) + A_2\cos(3\omega t - \varphi_3) \\ y_1 &= B_1\sin(\omega t - \varphi_1)\, B_2\sin(3\omega t - \varphi_3) \end{aligned} \tag{38}$$

we get

$$\begin{aligned} &A_1(\omega_0^2 - \omega^2)\cos(\omega t - \varphi_1) - 2h\omega A_1\sin(\omega t - \\ &\varphi_1) + A_2(\omega_0^2 - 9\omega^2)\cos(3\omega t - \varphi_3) - \\ &6h\omega A_2\sin(3\omega t - \varphi_3) \\ &= \frac{A_0^3}{4}[d_0\cos(\omega t - \varphi_0) - d_1\sin(\omega t - \varphi_0) + \\ &d_2\cos 3(\omega t - \varphi_0) - d_3\sin 3(\omega t - \varphi_0)] \\ &B_1(\omega_0^2 - \omega^2)\sin(\omega t - \varphi_1) + \\ &2h\omega B_1\cos(\omega t - \varphi_1) + B_2(\omega_0^2 - \\ &9\omega^2)\sin(3\omega t - \varphi_3) + \\ &+6h\omega B_2\cos(3\omega t - \varphi_3) = \frac{A_0^3}{4}[d_0\sin(\omega t - \\ &\varphi_0) + d_1\cos(\omega t - \varphi_0) + d_2\sin 3(\omega t - \end{aligned} \tag{39}$$

$\varphi_0) + d_3\cos3(\omega t - \varphi_0)]$

where

$e_0 = \omega_0^2 - \omega^2, d_0 = 3(k_1 + \omega^2 k_5) + k_2 + \omega^2 k_6, d_1 = \omega(k_3 + 3k_4 - k_7),$
$d_2 = k_1 + \omega^2 k_5 - (k_2 + \omega^2 k_6), d_3 = \omega(k_3 + k_4 - k_7).$

It is convenient to solve the system of Eq. (39) using the method of complex amplitudes. Then the system of Eq. (39) will take the form

$$\begin{aligned} &A\_1\,[(\omega\_0\hat{}2 - \omega\hat{}2) + 2ih\omega]e\hat{}(i(\omega t - \varphi\_1)) + A\_2\,[(\omega\_0\hat{}2 - 9\omega\hat{}2)) + 6ih\omega]e\hat{}(i(3\omega t - \varphi\_3)) = \\ &= \frac{A_0^3}{4[(d_0+id_1)e^{i(\omega t-\varphi_0)}+(d_2+id_3)e^{3i(\omega t-\varphi_0)}]} \\ &B_1[-i(\omega_0^2 - \omega^2) + 2h\omega]e^{i(\omega t-\varphi_1)} + B_2[-i(\omega_0^2 - 9\omega^2) + 6h\omega]e^{i(3\omega t-\varphi_3)} = \\ &= \frac{A_0^3}{4[(-id_0+d_1)e^{i(\omega t-\varphi_0)}+(-id_2+d_3)e^{3i(\omega t-\varphi_0)}]} \end{aligned} \quad (40)$$

Equating the coefficients of the functions $e^{i\omega t}$ and $e^{3i\omega t}$, after some calculations, we find the amplitude and the phase of the vibrations A_1

$$\begin{aligned} &A_1 = \frac{A_0^3\sqrt{d_0^2+d_1^2}}{4\sqrt{(\omega_0^2-\omega^2)^2+4h^2\omega^2}} \\ &tg(\varphi_1 - \varphi_0) = \frac{2h\omega d_0 - e_0 d_1}{e_0 d_0 + 2h\omega d_1}, \varphi_1 = arctg\left(\frac{2\omega h}{e_0}\right) + arctg\left(\frac{2h\omega d_0 - e_0 d_1}{e_0 d_0 + 2h\omega d_1}\right). \end{aligned} \quad (41)$$

Similarly, solving Eq. (39), we find the amplitude A_2 and phase φ_3 of the rotor vibrations.

$$\begin{aligned} &A_2 = \frac{A_0^3\sqrt{d2_2+d_3^2}}{4\sqrt{(\omega_0^2-9\omega^2)^2+36h^2\omega^2}}, \\ &tg(\varphi_3 - 3\varphi_0) = \frac{6h\omega d_2 - e_1 d_3}{e_1 d_2 + 6h\omega d_3}, \varphi_3 = 3arctg\left(\frac{2\omega h}{e_0}\right) + arctg\left(\frac{6h\omega d_2 - e_1 d_3}{e_1 d_2 + 6h\omega d_3}\right), \end{aligned} \quad (42)$$

Where $e_1 = \omega_0^2 - 9\omega^2$. Thus, the approximate law of rotor vibrations in the case of ultraharmonic vibrations is written as

$$\begin{aligned} &x = A_0\cos(\omega t - \varphi_0) + A_1\cos(\omega t - \varphi_1) + A_2\cos(3\omega t - \varphi_3), \\ &y = A_0\,sin(\,\omega t - \varphi_0) + A_1\,sin(\,\omega t - \varphi_1) + A_2\,sin(\,3\omega t - \varphi_3). \end{aligned} \quad (43)$$

The amplitude graphs for ultraharmonic vibrations with varying values of ω_0, d, c_1 and f are shown in Figs. 14-17.

2.2.4 Subharmonic vibrations

Let us consider the case when the rotor performs forced and subharmonic vibrations. This is the case as the nonlinear differential equations of motion (7) contain a cubic nonlinear term proportional to k_1x^3, k_1y^3, *i.e.* the Duffing-type equations. Therefore, it can be assumed that in the considered rotor system, subharmonic vibrations may arise, the frequency of which is two, three and more times less than the frequency of the disturbing force and ultra harmonic vibrations, the frequency of which is two, three and more times greater than the frequency of the disturbing force. We will assume that the forced vibrations of the rotor are superimposed by subharmonic vibrations with a frequency of $\omega/2$. Let us consider the use of the method of the imaging function in the study of forced and subharmonic vibrations of the rotor. Then the rotor motion can be represented as

$$\begin{aligned} &x = a_1\cos(\omega t - \varphi_1) + a_2\cos\left(\frac{1}{2}\omega t - \varphi_2\right), \\ &y = a_1\sin(\,\omega t - \varphi_1) + a_2\sin\left(\frac{1}{2}\omega t - \varphi_2\right). \end{aligned} \quad (44)$$

Substituting expressions (44) into the left side of the equation of rotor motion (7), we obtain

$$\begin{aligned} &a_1\left\{4(\omega_0^2 - \omega^2) - \left[3k_1(a_1^2 + 2a_2^2) + k_2(a_1^2 + 2a_2^2) + \omega^2 k_5\left(3a_1^2 + \frac{5}{2}a_2^2\right) + \omega^2 k_6\left(a_1^2 + \frac{1}{2}a_2^2\right)\right]\right\}\cos(\omega t - \varphi_1) + \\ &+a_2\{4(\omega_0^2 - \tfrac{1}{4}\omega^2) - [3k_1(2a_1^2 + a_2^2) + k_2(2a_1^2 + a_2^2) + \omega^2 k_5(4a_1^2 + \tfrac{3}{4}a_2^2) + \omega^2 k_6(2a_1^2 + \\ &+\tfrac{1}{4}a_2^2)]\}\cos\left(\tfrac{1}{2}\omega t - \varphi_2\right) + \omega\{a_1[(k_3 + 3k_4 - k_7)a_1^2 + (2k_3 + 4k_4 - k_7)a_2^2) \\ &-8h]\,sin(\,\omega t - \varphi_1) + a_2[3k_3(a_1^2 + \tfrac{1}{2}a_2^2) + k_4(5a_1^2 + \tfrac{3}{2}a_2^2) - k_7(2a_1^2 + \tfrac{1}{2}a_2^2) - \\ &-2h]\,sin(\tfrac{1}{2}\omega t - \varphi_2)\} + a_1^2 a_2(3k_1 + k_2 + 2\omega^2 k_5)\cos\left(\tfrac{3}{2}\omega t - 2\varphi_1 + \varphi_2\right) + a_1 a_2^2[3k_1 + k_2 + \\ &+\tfrac{\omega^2}{4}(5k_5 + 3k_6)]\cos(-\varphi_1 + 2\varphi_2) + a_2^3[(k_1 - k_2 + \tfrac{\omega^2}{4}(k_5 - k_6)](\tfrac{3}{2}\omega t - 3\varphi_2)] + \\ &\ldots. \end{aligned} \quad (45)$$

Replacing in expression (45) the *cosine* with the *sine*, and the *sine* with the *cosine* with the same arguments, we obtain the equation along the *Oy* axis, which is completely identical to (45). According to the method of the image function, it is permissible to use a complex notation, and then Eq. (45) can be written as:

$$\begin{aligned} &a_1[\delta_0 - (\delta_1 a_1^2 + \delta_2 a_2^2) - i(\delta_3 a_1^2 + \delta_4 a_2^2 - 8h)]e^{i(\omega t-\varphi_1)} + [\chi_0 - (\chi_1 a_1^2 + \chi_2 a_2^2) - \\ &-i(\chi_3 a_1^2 + \chi_4 a_2^2 - 2h)]e^{i\left(\frac{1}{2}\omega t-\varphi_2\right)} + \\ &\eta_0 e^{i\left(\frac{3}{2}\omega t-2\varphi_1+\varphi_2\right)} + \eta_1 e^{i\left(\frac{3}{2}\omega t-3\varphi_2\right)} + \\ &\eta_2 e^{i(2\varphi_2-\varphi_1)} + \ldots \end{aligned} \quad (46)$$

where

$\delta_0 = 4(\omega_0^2 - \omega^2), \delta_1 = (3k_1 + k_2) + \omega^2(3k_5 + k_6), \delta_2 = 2(3k_1 + k_2) + \frac{1}{2}\omega^2(5k_5 + k_6),$

$\delta_3 = \omega(k_3 + 3k_4 - k_7), \delta_4 = \omega(2k_3 + 4k_4 - k_7), \chi_o = 4\left(\omega_0^2 - \frac{1}{4}\omega^2\right), \chi_1 = 2\left[(3k_1 + k_2) + \omega^2\,(2k_5 + k_6)\right],$
$\chi_2 = (3k_1 + k_2) + \frac{1}{4}\omega^2(3k_5 + k_6), \chi_3 = \omega(k_3 + 3k_4 - 2k_7), \chi_4 = \omega\left(2k_3 + 4k_4 - \frac{1}{2}k_7\right),$
$\eta_0 = a_1^2 a_2[3k_1 + k_2 + 2\omega^2 k_5], \eta_1 = a_2^3\left[k_1 - k_2 + \frac{1}{4}\omega^2(k_5 - k_6)\right], \eta_2 = a_1 a_2^2\left[3k_1 + k_2 + \frac{1}{4}\omega^2(5k_5 + 3k_6)\right].$

As a result, we obtain a two-frequency imaging function

$$\begin{aligned} &E_1(\omega, a_1, a_2) = 4(\omega_0^2 - \omega^2) - [(3k_1 + k_2) + \omega^2(3k_5 + k_6)]a_1^2 - \left[2(3k_1 + k_2) + \frac{1}{2}\omega^2(5k_5 + k_6)\right]a_2^2 - i\omega[(k_3 + 3k_4 - k_7)a_1^2 + (2k_3 + 4k_4 - k_7)a_2^2 - 8h], \\ &E_2(\omega, a_1, a_2) = 4\left(\omega_0^2 - \frac{1}{4}\omega^2\right) - 2[(3k_1 + k_2) + \omega^2(3k_5 + k_6)]a_1^2 - \left[2(3k_1 + k_2) + \frac{1}{2}\omega^2(5k_5 + k_6)\right]a_2^2 - i\omega[(k_3 + 3k_4 - k_7)a_1^2 + \omega(2k_3 + 4k_4 - k_7)a_2^2 - 2h] \end{aligned} \quad (47)$$

Substituting the disturbing force into the first equation of system (47), we get

$$\begin{aligned} &a_1[\delta_0 - (\delta_1 a_1^2 + \delta_2 a_2^2) - i(\delta_3 a_1^2 + \delta_4 a_2^2 - 8h)] = 2fe^{i\varphi_1}, \\ &\chi_0 - (\chi_1 a_1^2 + \chi_2 a_2^2) - i(\chi_3 a_1^2 + \chi_4 a_2^2 - 2h) = 0, \\ &2f = me\omega^2. \end{aligned} \quad (48)$$

Separating the real and imaginary parts in system (48) and taking into account only the real parts, and then setting $\varphi_1 = 0,\ h = 0$, we obtain a reduced cubic equation

$$a_1^3 + p_5 a_1 + q_5 = 0, \quad (49)$$

where

$p_5 = \frac{\theta_1}{\theta_0}, q_5 = \frac{2f}{\theta_0}, \xi_0 = \frac{\chi_0}{\chi_2}, \xi_1 = \frac{\chi_1}{\chi_2}, \theta_0 = \delta_1 - \delta_2\xi_1, \theta_1 = \delta_2\xi_0 - \delta_0.$

The roots of Eq. (49) are determined by Cardano's formulas. The unknown amplitude a_2 is determined from (48) in the form $a_2^2 = \xi_0 - \xi_1 a_1^2$. To determine the dynamic dependence of the amplitude of the main vibrations, *i.e.* forced vibrations with the amplitude of the subharmonic vibrations of the rotor, we require that

$$\Delta(t) = \eta_0 e^{i\left(\frac{3}{2}\omega t - 2\varphi_1 + \varphi_2\right)} + \eta_1 e^{i\left(\frac{3}{2}\omega t - 3\varphi_2\right)} + \eta_2 e^{i(2\varphi_2 - \varphi_1)} = 0. \quad (50)$$

Then, in (50), taking into account that $\varphi_1 = 0$, we obtain

$$a_1^2[3k_1 + k_2 + 2\omega^2 k_5]e^{i\frac{3}{2}\omega t} + a_2^2\left[k_1 - k_2 + \frac{1}{4}\omega^2(k_5 - k_6)\right]e^{i\left(\frac{3}{2}\omega t - 4\varphi_2\right)} + a_1 a_2\left[3k_1 + k_2 + \frac{\omega^2}{4}(5k_5 + 3k_6)\right]e^{i\varphi_2} = 0. \quad (51)$$

After expanding the terms of the exponential function $\cos(3\omega t - 4\varphi_2)$ and equating the coefficients at $\sin\frac{3\omega t}{2}$ to zero, we get

$$\sin 4\varphi_2 = 0, \varphi_2 = \frac{\pi}{4}, \cos\varphi_2 = \frac{\sqrt{2}}{2}.$$

We assume that $sin\,4\varphi_2 = 0.4\varphi_2 = \pi,\ a_2 \gg a_1$. Then from (51) we get

$$a_1 = \frac{\sqrt{2}[k_1 - k_2 + \frac{1}{4}\omega^2(k_5 - k_6)]a_2}{[3k_1 + k_2 + \frac{\omega^2}{4}(5k_5 + 3k_6)]}\cos\frac{3\omega t}{2}. \quad (52)$$

Expression (52) has the following meaning. If we take into account that a_1 is the amplitude of the rotor vibrations at a frequency equal to the rotor rotation frequency, then the rotor motion turns into a circular synchronous precession, as during subharmonic vibrations of the rotor another frequency is superimposed on the main vibrations. The precession will not be circular and the center of the spike will describe three complete vibrations about the static equilibrium position in two rotor revolutions. In this case the rotor precession frequency is equal to $\frac{3}{2}\omega$. The graphs of the amplitudes for the case of subharmonic vibrations with variations in the values of ω_0, d, c_1 and f are shown in Figs. 18-21.

2.2.5 Self-excited vibrations

Let us consider the following case, when the rotor performs forced vibrations and self-excited vibrations simultaneously. Such a rotor motion can be expected naturally, as the system is nonlinear. In this case, the solution to the system of Eq. (7) is represented as

$$z = x + iy = ae^{i\omega t} + be^{i\Omega t} \quad (53)$$

The first terms in Eq. (53) define the forced vibrations of the rotor with the amplitude a and frequency ω, and the second terms define the self-vibrations with the amplitude b and frequency Ω. Substituting (53) into the equation of rotor motion (7), including the phase angle φ in the expression for the disturbing force, and then equating the coefficients at the time functions, we get

$$\begin{aligned} &a\{4(\omega_0^2 - \omega^2) - [(3k_1 + k_2)(a^2 + 2b^2) + k_5(3\omega^2 a^2 + 2\Omega(2\omega + \Omega)b^2) + k_6(\omega^2 a^2 + 2\Omega^2 b^2)]\} = 8f cos\varphi \\ &a\{k_3\omega(a^2 + 2b^2) + k_4[3\omega a^2 + 2(\omega + 2\Omega)b^2] - k_7(\omega a^2 + 2\Omega b^2) - 8h\omega\} = 8f\,sin\,\varphi \\ &4(\omega_0^2 - \Omega^2) - [(3k_1 + k_2)(b^2 + 2a^2) + k_5(3\Omega^2 b^2 + 2\omega(2\Omega + \omega)a^2) + k_6(\Omega^2 b^2 + 2\omega^2 a^2)] = 0 \\ &k_3\Omega(b^2 + 2a^2) + k_4[3\Omega b^2 + 2(\Omega + 2\omega)a^2] - k_7(\Omega b^2 + 2\omega a^2) = 8h\Omega \end{aligned} \quad (54)$$

We obtain exactly the same equations from the second equation of system (7). Therefore, it is sufficient to solve a nonlinear algebraic system of equations for the unknowns a, b, Ω, φ. After collecting the terms for a^2 and b^2, system (54) takes the form

$$\begin{aligned} &a(g_0 - g_1a^2 - g_2b^2) = 8f\cos\varphi \\ &a(g_3a^2 + g_4b^2 - d_0) = 8f\sin\varphi \\ &g_5 - g_6a^2 - g_7b^2 = 0 \\ &g_8a^2 + g_9b^2 = d_1 \end{aligned} \tag{55}$$

where

$$\begin{aligned} &g_0 = 4(\omega_0^2 - \omega^2), g_1 = 3k_1 + k_2 + \omega^2(3k_5 + k_6), g_2 = 2[3k_1 + k_2 + (\Omega^2 + 2\Omega\omega)k_5 + \Omega^2k_6], \\ &g_3 = \omega(k_3 + 3k_4 - k_7), g_4 = 2[\omega k_3 + (\omega + 2\Omega)k_4 - \Omega k_7], d_0 = 8h\omega, g_5 = 4(\omega_0^2 - \Omega^2), \\ &g_6 = 2[3k_1 + k_2 + (\omega^2 + 2\Omega\omega)k_5 + \omega^2k_6], g_7 = 3k_1 + k_2 + \Omega^2(3k_5 + k_6), d_1 = 8h\Omega, \\ &g_8 = 2[\Omega k_3 + (\Omega + 2\omega)k_4 - \omega k_7], g_9 = \Omega(k_3 + 3k_4 - k_7). \end{aligned} \tag{56}$$

Excluding the phase angle φ from the first two equations of system (55), we find

$$a^2[(g_0 - g_1a^2 - g_2b^2)^2 + (g_3a^2 + g_4b^2 - d_0)^2] = 64f^2 \tag{57}$$

Dividing the second equation of system (55) by the first, we obtain an expression for the vibration phase φ

$$\varphi = \operatorname{arctg}\left(\frac{g_3a^2 + g_4b^2 - d_0}{g_0 - g_1a^2 - g_2b^2}\right) \tag{58}$$

From the third and fourth equations of system (55), the squares of the amplitudes of forced vibrations and self-excited vibrations of the rotor a^2 and $b^2$are determined.

$$a^2 = \frac{d_1g_7 - g_5g_9}{g_7g_8 - g_6g_9}, b^2 = \frac{g_5g_8 - d_1g_6}{g_7g_8 - g_6g_9}. \tag{59}$$

Substituting (59) into (57) and taking (56) into account, we obtain an equation for Ω (the frequency of self-excited vibrations of the rotor) in the form

$$\begin{aligned} &G_0\Omega^{13} + G_1\Omega^{12} + G_2\Omega^{11} + G_3\Omega^{10} + G_4\Omega^9 + \\ &G_5\Omega^8 + G_6\Omega^7 + G_7\Omega^6 + G_8\Omega^5 + G_9\Omega^4 + \\ &G_{10}\Omega^3 + G_{11}\Omega^2 + G_{12}\Omega + G_{13} = 0 \end{aligned} \tag{60}$$

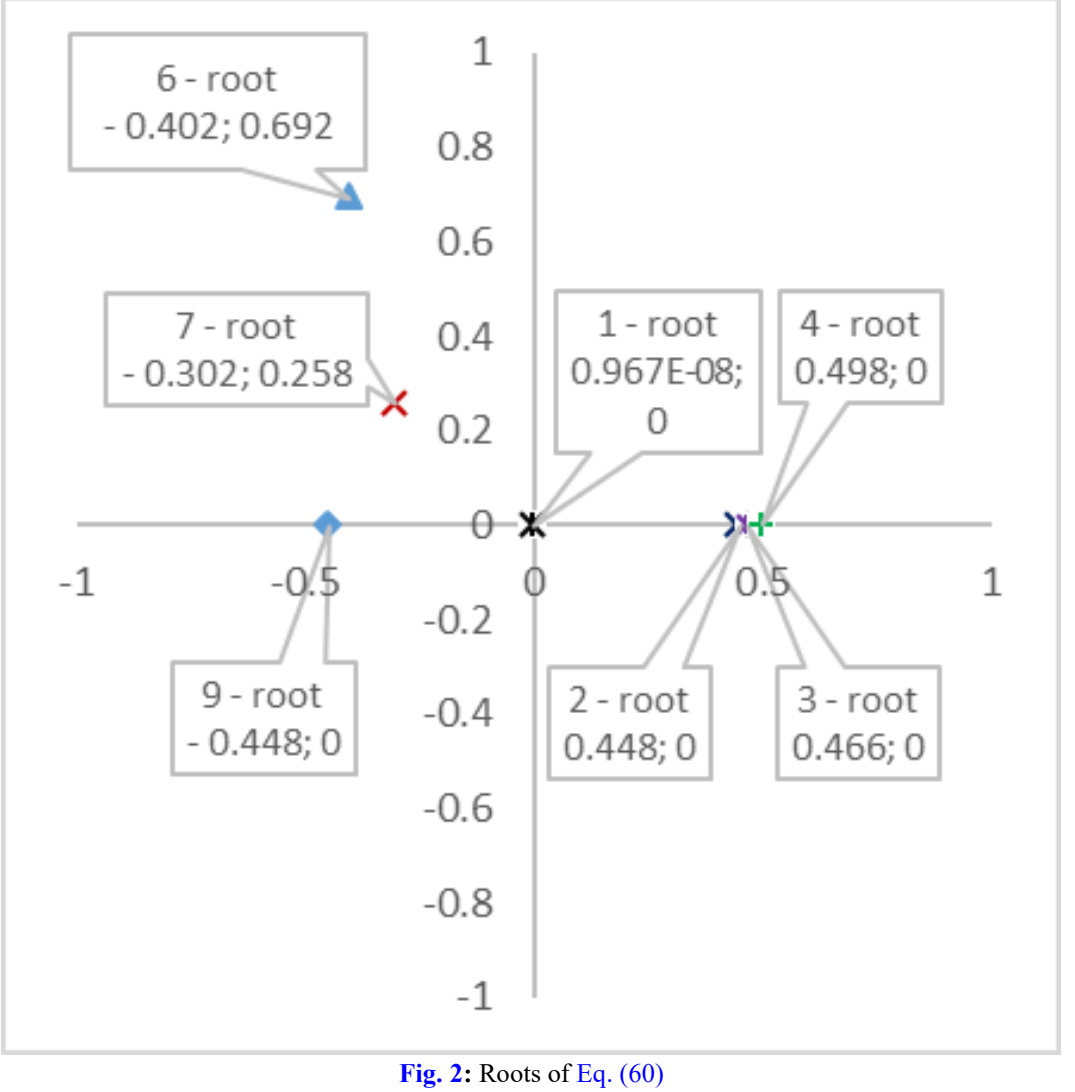

Fig. 2: Roots of Eq. (60)

where

$$G_0 = \eta_0\delta_0, G_1 = \eta_0\delta_1, G_2 = \eta_0\lambda_0 + \eta_1\delta_0, G_3 = \eta_0\lambda_1 + \eta_1\delta_1, G_3 = \eta_0\lambda_1 + \eta_1\delta_1,$$
$$G_4 = \eta_0\lambda_2 + \eta_1\lambda_0 - f_0\sigma_0, G_4 = \eta_0\lambda_2 + \eta_1\lambda_0 - f_0\sigma_0, G_4 = \eta_0\lambda_2 + \eta_1\lambda_0 - f_0\sigma_0,$$
$$G_5 = \eta_0\lambda_3 + \eta_1\lambda_1 - f_0\sigma_1, G_6 = \eta_0\lambda_4 + \eta_1\lambda_2 - f_0\sigma_2, G_7 = \eta_0\lambda_5 + \eta_1\lambda_3 - f_0\sigma_3,$$
$$G_8 = \eta_0\lambda_6 + \eta_1\lambda_4 - f_0\sigma_4, G_9 = \eta_0\lambda_7 + \eta_1\lambda_5 - f_0\sigma_5, G_{10} = \eta_0\lambda_8 + \eta_1\lambda_6 - f_0\sigma_6,$$
$$G_{11} = \eta_1\lambda_7 - f_0\sigma_7, G_{12} = \eta_1\lambda_8 - f_0\sigma_8, G_{13} = -f_0\sigma_9.$$

$$\eta_0 = l_2\chi_7 + 4\chi_{11}, \eta_1 = l_2\chi_8 - l_0\chi_1, \eta_2 = \chi_7\chi_9, \eta_3 = \chi_7\chi_{10} - \chi_5\chi_{11}, \eta_4 = \chi_8\chi_9 - \chi_6\chi_{11}, \eta_5 = \chi_8\chi_{10},$$

$$l_0 = 4\omega_0^2, l_1 = 8f, l_2 = 8h, f_0 = 64f^2.$$

$$\chi_2 = 2(3k_1 + k_2), \chi_4 = 2\omega(k_3 + k_4), \chi_5 = 4\omega k_5,$$
$$\chi_6 = 2[(3k_1 + k_2) + \omega^2(k_5 + k_6)], \chi_7 = 3k_5 + k_6, \chi_8 = 3k_1 + k_2,$$
$$\chi_9 = 2(k_3 + k_4), \chi_{10} = 2\omega(2k_4 - k_7), \chi_{11} = k_3 + 3k_4 - k_7.$$

$$\delta_0 = j_1\gamma_0^2, \delta_1 = 2j_1\gamma_0\gamma_1 + j_2\gamma_0^2, \delta_2 = j_1(\gamma_1^2 + 2\gamma_0\gamma_2) + 2j_2\gamma_0\gamma_1 + j_3\gamma_0^2,$$
$$\delta_3 = 2j_1(\gamma_0\gamma_3 + \gamma_1\gamma_2) + j_2(\gamma_1^2 + 2\gamma_1\gamma_3) + 2j_3\gamma_0\gamma_1 + j_4\gamma_0^2,$$
$$\delta_4 = j_1(\gamma_2^2 + 2\gamma_1\gamma_3) + 2j_1(\gamma_0\gamma_3 + \gamma_1\gamma_2) + j_3(\gamma_1^2 + 2\gamma_0\gamma_2) + 2j_4\gamma_0\gamma_1 + j_5\gamma_0^2,$$
$$\delta_5 = 2j_1\gamma_2\gamma_3 + j_2(\gamma_2^2 + 2\gamma_1\gamma_3) + 2j_3(\gamma_0\gamma_3 + \gamma_1\gamma_2) + j_4(\gamma_1^2 + 2\gamma_0\gamma_2) + 2j_5\gamma_0\gamma_1,$$
$$\delta_6 = j_1\gamma_3^2 + 2j_2\gamma_2\gamma_3 + j_3(\gamma_2^2 + 2\gamma_1\gamma_3) + 2j_4(\gamma_0\gamma_3 + \gamma_1\gamma_2) + j_5(\gamma_1^2 + 2\gamma_0\gamma_2),$$
$$\delta_7 = j_2\gamma_3^2 + 2j_3\gamma_2\gamma_3 + j_4(\gamma_2^2 + 2\gamma_1\gamma_3) + 2j_5(\gamma_0\gamma_3 + \gamma_1\gamma_2),$$
$$\delta_8 = j_3\gamma_3^2 + 2j_4\gamma_0\gamma_3 + j_5(\gamma_2^2 + 2\gamma_1\gamma_3), \delta_9 = j_4\gamma_3^2 + 2j_5\gamma_2\gamma_3, \delta_{10} = j_5\gamma_3^2.$$

$$j_0 = [3k_1 + k_2 + \omega^2(3k_5 + k_6)]^2 + \omega^2(k_3 + 3k_4 - k_7)^2, j_1 = \chi_0^2, j_2 = 2\chi_0\chi_1,$$
$$j_3 = \chi_1^2 + 2\chi_0\chi_2 + \chi_3^2, j_4 = 2(\chi_1\chi_2 + \chi_3\chi_4), j_5 = \chi_2^2 + 2\chi_0\chi_2 + \chi_4^2, j_6 = 2g_1\chi_0,$$
$$j_7 = 2(g_1\chi_1 + g_3\chi_3), j_8 = 2(g_1\chi_2 + g_3\chi_4), j_9 = -2(g_0g_1 + d_0g_3), j_{10} = -2g_0\chi_0,$$
$$j_{11} = -2(g_0\chi_1 - d_0\chi_3), j_{12} = -2(g_0\chi_2 - d_0\chi_4), j_9 = -2(g_0g_1 + d_0g_3), d_0 = 8h\omega.$$

$$\gamma_0 = -4\chi_9, \gamma_1 = -(4\chi_{10} + l_2\chi_5), \gamma_2 = l_0\chi_9 - l_2\chi_6, \gamma_3 = l_0\chi_9. \tag{61}$$

$$\lambda_0 = \delta_2 + \theta_0 + \pi_0, \lambda_1 = \delta_3 + \theta_1 + \pi_1, \lambda_2 = \delta_4 + \theta_2 + \pi_2 + j_0\nu_0 + j_9\xi_0 + e_0\nu_3$$
$$\lambda_3 = \delta_5 + \theta_3 + \pi_3 + j_9\xi_1 + e_0\nu_4, \lambda_4 = \delta_6 + \theta_4 + \pi_4 + j_0\nu_1 + j_9\xi_2 + e_0\nu_5,$$
$$\lambda_5 = \delta_7 + \theta_5 + \pi_{5_2} + j_9\xi_3 + e_0\nu_6, \lambda_6 = \delta_8 + \theta_6 + \pi_6 + j_0\nu_2 + j_9\xi_4 + e_0\nu_7,$$
$$\lambda_7 = \delta_9 + \theta_7 + \pi_7 + j_9\xi_5 + e_0\nu_8, \lambda_8 = \delta_{10} + \pi_8 + e_0\nu_9, e_0 = g_0^2 + d_0^2.$$

$$\theta_0 = j_6\varepsilon_0, \theta_1 = j_6\varepsilon_1 + j_7\varepsilon_0, \theta_2 = j_6\varepsilon_2 + j_7\varepsilon_1 + j_8\varepsilon_0, \theta_3 = j_6\varepsilon_3 + j_7\varepsilon_2 + j_8\varepsilon_1,$$
$$\theta_4 = j_6\varepsilon_4 + j_7\varepsilon_3 + j_8\varepsilon_2, \theta_5 = j_6\varepsilon_5 + j_7\varepsilon_4 + j_8\varepsilon_3, \theta_6 = j_7\varepsilon_5 + j_8\varepsilon_4, \theta_7 = j_8\varepsilon_5,$$

$$\varepsilon_0 = \eta_0\gamma_0, \varepsilon_1 = \eta_0\gamma_1, \varepsilon_2 = \eta_0\gamma_2 + \eta_1\gamma_0, \varepsilon_3 = \eta_0\gamma_3 + \eta_1\gamma_1, \varepsilon_4 = \eta_1\gamma_2, \varepsilon_5 = \eta_1\gamma_3.$$

$$\pi_0 = j_{10}\zeta_0, \pi_1 = j_{10}\zeta_1 + j_{11}\zeta_0, \pi_2 = j_{10}\zeta_2 + j_{11}\zeta_1 + j_{12}\zeta_0, \pi_3 = j_{10}\zeta_3 + j_{11}\zeta_2 + j_{12}\zeta_1,$$
$$\pi_4 = j_{10}\zeta_4 + j_7\zeta_3 + j_8\zeta_2, \pi_5 = j_{10}\zeta_5 + j_{11}\zeta_4 + j_{12}\zeta_3, \pi_6 = j_{10}\zeta_6 + j_{11}\zeta_5 + j_{12}\zeta_4,$$
$$\pi_7 = j_{11}\zeta_6 + j_{12}\zeta_5, \pi_8 = j_{12}\zeta_6.$$

$$\zeta_0 = \eta_2\gamma_0, \zeta_1 = \eta_0\eta_3, \zeta_2 = \eta_2\gamma_2 + \eta_3\gamma_1 + \eta_4\gamma_0, \zeta_3 = \eta_2\gamma_3 + \eta_3\gamma_2 + \eta_4\gamma_1 + \eta_5\gamma_0,$$
$$\zeta_4 = \eta_3\gamma_3 + \eta_4\gamma_2 + \eta_5\gamma_1, \zeta_5 = \eta_4\gamma_3 + \eta_5\gamma_2, \zeta_6 = \eta_5\gamma_3.$$

$$\nu_0 = \eta_0^2, \nu_1 = 2\eta_0\eta_1, \nu_2 = \eta_1^2, \nu_3 = \eta_2^2, \nu_4 = 2\eta_2\eta_3, \nu_5 = \eta_3^2 + 2\eta_2\eta_4,$$
$$\nu_5 = \eta_3^2 + 2\eta_2\eta_4, \nu_6 = 2(\eta_2\eta_5 + \eta_3\eta_4), \nu_7 = \eta_4^2 + 2\eta_3\eta_5, \nu_8 = 2\eta_4\eta_5, \nu_9 = \eta_5^2.$$

$$\xi_0 = \eta_0\eta_2, \xi_1 = \eta_0\eta_3, \xi_2 = \eta_0\eta_4 + \eta_1\eta_2, \xi_3 = \eta_0\eta_5 + \eta_1\eta_3, \xi_4 = \eta_1\eta_4, \xi_5 = \eta_1\eta_5,$$

$$\sigma_0 = \eta_2\nu_3, \sigma_1 = \eta_2\nu_4 + \eta_3\nu_3, \sigma_2 = \eta_2\nu_5 + \eta_3\nu_4 + \eta_4\nu_3, \sigma_3 = \eta_2\nu_6 + \eta_3\nu_5 + \eta_4\nu_4 + \eta_5\nu_3,$$
$$\sigma_4 = \eta_2\nu_7 + \eta_3\nu_6 + \eta_4\nu_5 + \eta_5\nu_4, \sigma_5 = \eta_2\nu_8 + \eta_3\nu_7 + \eta_4\nu_6 + \eta_5\nu_5, \sigma_5 = \eta_2\nu_8 + \eta_3\nu_7 + \eta_4\nu_6 + \eta_5\nu_5$$
$$\sigma_6 = \eta_2\nu_9 + \eta_3\nu_8 + \eta_4\nu_7 + \eta_5\nu_6, \sigma_7 = \eta_3\nu_9 + \eta_4\nu_8 + \eta_5\nu_7, \sigma_8 = \eta_4\nu_9 + \eta_5\nu_8, \sigma_9 = \eta_5\nu_9.$$

In the general case, Ω is a complex number, the real part of which defines the degree of intensity of self-excited vibrations, and the imaginary part – the degree of instability of the rotor system. Slowly changing the rotation frequency of the centrifuge ω over a wide range with fixed values of the remaining rotor parameters and parameters of the magnetic bearings, we obtained the dependences of the frequency of self-excited vibrations Ω on the angular velocity of the rotor ω, *i.e.*, curves in the plane (ω, Ω), (see Figs. 26-28). The instability zones of the GCMB correspond to those values of the angular velocity of the rotor at which Eq. (60) has complex roots with a negative imaginary part (see Fig. 2). As can be seen, the stability zones correspond to the values of the angular velocity of the rotor for the first four roots of Eq. (60). As the lowest frequency is usually taken as the first, the study based on parametric analysis was made for the first root of Eq (60). Then, also smoothly changing the rotation frequency of the centrifuge ω at a known frequency of self-excited vibrations (natural frequency) Ω according to formula (59), we find the amplitudes of forced and self-excited vibrations of the rotor when varying the parameters of the rotor system. Based on the found values, it is possible to construct curves of the dependences of the amplitude of forced and self-excited vibrations of the rotor on the angular velocity of the centrifuge $(\omega, a), (\omega, b)$ for different values of the centrifuge parameters and parameters of the magnetic bearings of the rotor system. We constructed the amplitude-frequency responses (AFR) of the rotor system in the plane $(\omega, a), (\omega, b)$. Using the dependence of the amplitude-frequency responses on changes in the rotor parameters and parameters of magnetic bearings (mass, current and other parameters), we can select those values of the rotor system parameters at which the amplitudes of forced vibrations and self-excited vibrations are significantly reduced, and the width of the zones of self-excited vibrations of the rotor system is narrowed or the zone of self-excited vibrations disappears.

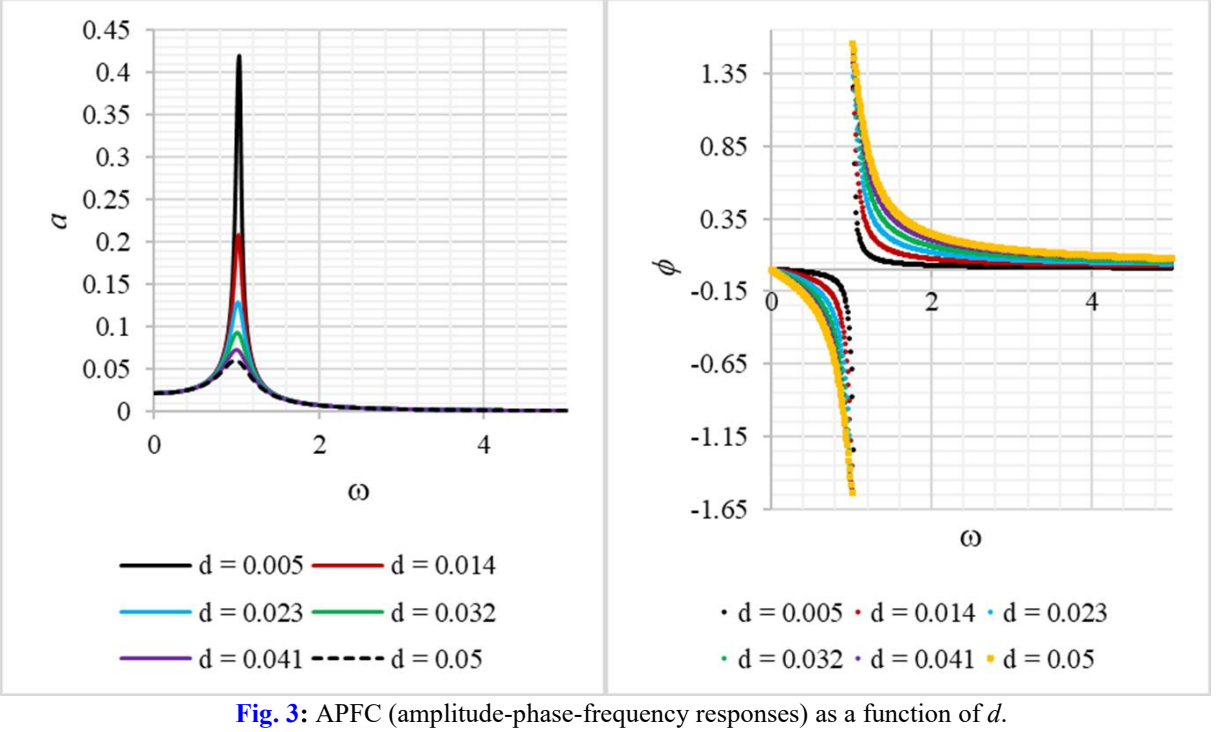

Fig. 3: APFC (amplitude-phase-frequency responses) as a function of *d*.

3. Results and discussion

For the simplest case of forced vibrations, *i.e.* when the shaft center performs a circular precession motion around the equilibrium position, the amplitude-phase frequency characteristics were constructed for the cubic Eq. (19). The variables *d*, c_1 and *f* were chosen as variable parameters (see Eq. 9). It was assumed that $p = 1.22$, $\alpha = 22.5^{o}$. An analysis of the amplitude and phase-frequency characteristics when varying the coefficient *d* in the PD controller shows that an increase in this parameter leads to a significant decrease in the amplitude of resonant vibrations (see Fig. 3). When changing *d* from 0.005 to 0.05, a decrease in the amplitude by more than 4 times is observed, which confirms the pronounced damping effect of the controller (see Fig. 3, left). However, the resonance frequency ($\omega \approx 1.03$) remains almost constant, which indicates that *d* only affects the amplitude, but does not shift the natural frequency of the system. This corresponds to the behavior of linear or weakly nonlinear vibratory systems.

The phase plot shows that at low *d* values the system exhibits a sharp phase transition, while at higher *d* the phase changes more smoothly (see Fig. 3, right). This indicates that increasing *d* makes the system response more stable and less sensitive to resonant disturbances. A smoother phase transition also indicates a decrease in the response inertia and a decrease in the phase lag between the input and the system response. Thus, an increase in the *d*-factor increases the stability of the system, smoothes the phase characteristic and suppresses the amplitude of vibrations without affecting the resonant frequency. This makes a PD controller with a large *d*-value especially effective for active suppression of vibrations in

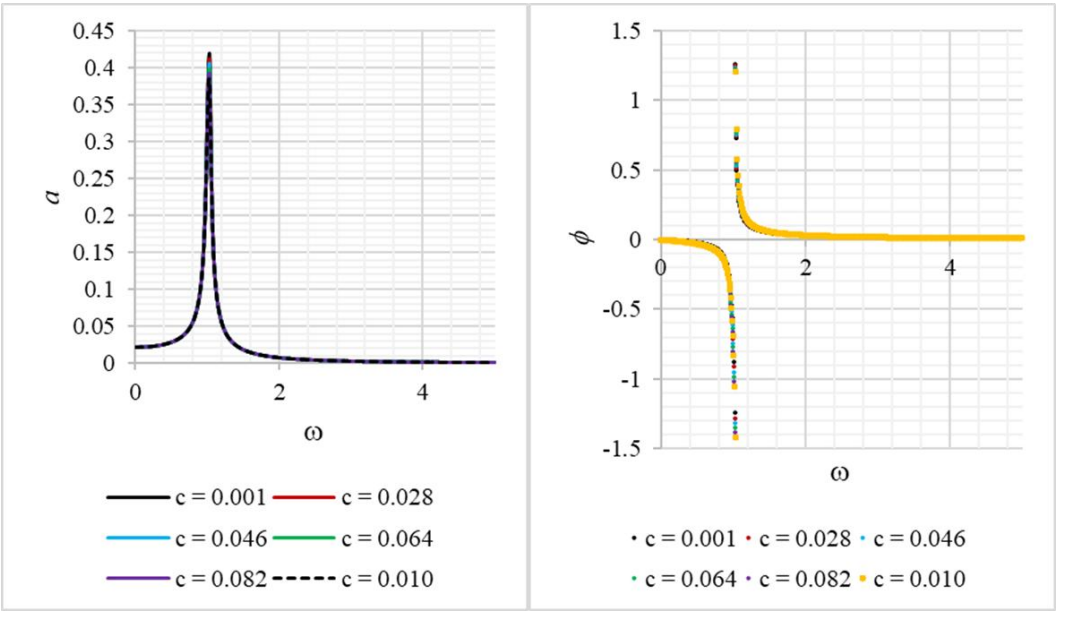

Fig. 4: Amplitude-frequency response as a function of c_1.

magnetic suspensions. In engineering practice, this allows for more accurate control of the rotor position and minimization of dynamic deviations, especially near the resonant modes.

Variations in the parameter c_1 have little effect on the dynamics of the amplitudes as a whole, which is shown in detail in Fig. 4. An analysis of the amplitude and phase-frequency characteristics with variation of the air gap c_1 shows that this parameter has a minimal effect on the behavior of the system in the steady state. In the amplitude characteristic, all curves, including those obtained at extreme values of c_1 from 0.001 to 0.082, practically overlap each other (Fig. 4, the left graph), which indicates an insignificant change in the amplitude of resonant vibrations. Even an increase in the gap by tens of times leads to a decrease in the amplitude by less than 1%, which is a negligible effect in the context of control. The phase characteristic also demonstrates almost complete coincidence of the phase curves for different values of c_1 (Fig. 4, the right graph). This means that changes in the air gap do not affect the phase response of the system, and do not cause delays or phase shifts in the operating frequency range. In addition, the frequency of the resonant peak ($\omega \approx 1.03$) remains unchanged in all cases, which confirms the stability of the natural frequency of the system under gap changes. Thus, it can be concluded that the parameter c_1 (steady-state air gap) does not have a significant effect on the amplitude-phase characteristics of the system under normal conditions. This is explained by the fact that in the model of magnetic suspension the gap affects the rigidity and the force of attraction, but in the steady state with small disturbances its influence is weakly expressed. This result is useful in practice, as it allows variations in the gap without deterioration of stability or appearance of undesirable resonance effects.

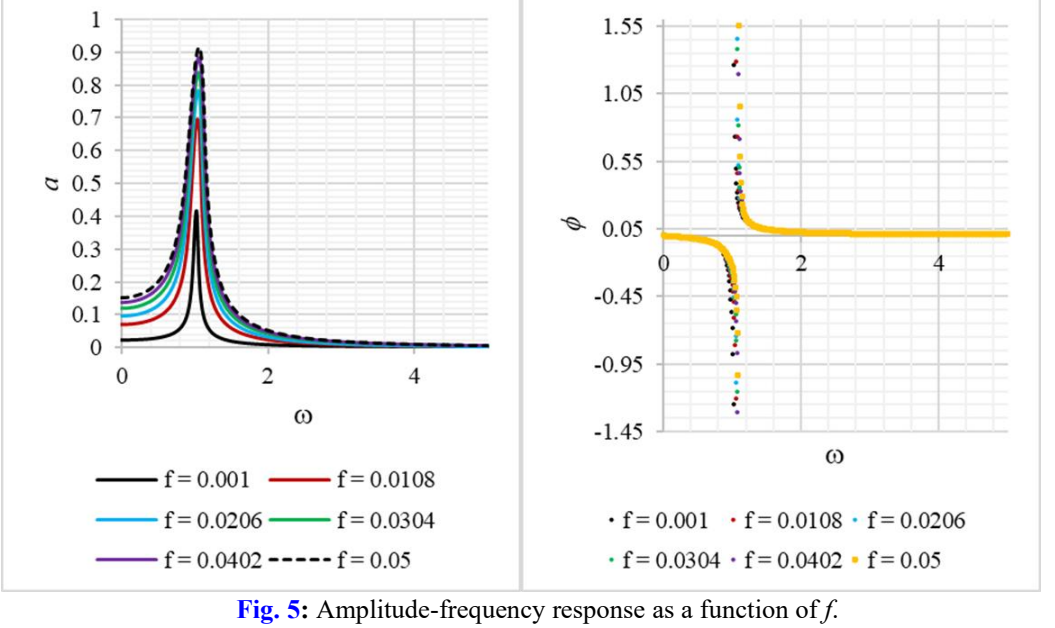

Fig. 5: Amplitude-frequency response as a function of f.

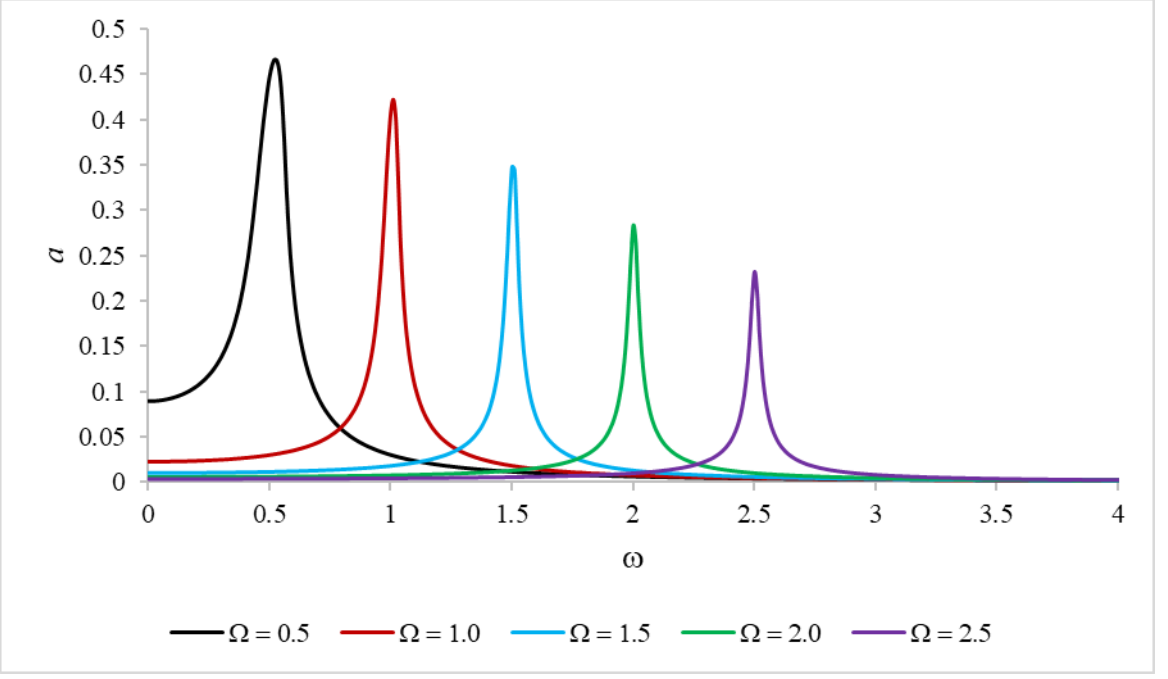

Fig. 6: Amplitude-frequency response as a function of frequency Ω.

An analysis of the graphs shows that an increase in the rotor eccentricity *f* leads to a significant increase in the vibrations amplitude *a*, especially in the region of the resonant frequency. The amplitude-frequency characteristic (Fig. 5, left graph) shows that with an increase in *f* from 0.001 to 0.05, the amplitude increases almost 2.5 times, from 0.4 to 0.9, which indicates a high sensitivity of the system to the displacement of the center of mass. At the same time, the position of the resonant frequency ω remains almost constant (about 1.03), indicating the absence of a noticeable frequency shift with a moderate increase in *f*. The phase-frequency characteristic (Fig. 5, right graph) demonstrates small differences between the curves at different *f* values. All curves undergo the same phase transition from -π/2 to +π/2, and their shape is almost independent of the eccentricity value. This indicates that *f* primarily affects the excitation force and amplitude, but not the phase structure of the system response. It means that the eccentricity *f* plays a key role in the formation of resonant amplitudes. Even small rotor displacements can cause a sharp increase in vibrations, which is especially critical when operating near the resonant frequency. At the same time, the phase response and the frequency position of the peak remain stable.

This emphasizes the need for rotor balancing in centrifuge installations: high amplitude with small *f* can lead to destructive vibrations. The amplitude control in this case is only possible through active damping, as a decrease in *f* directly reduces excitation.

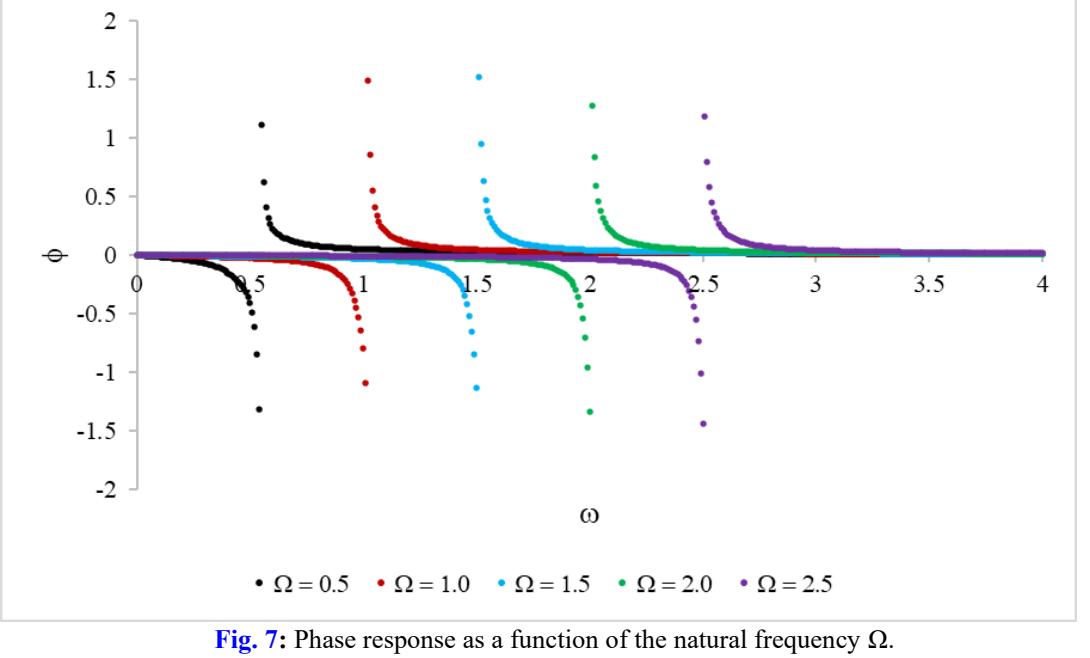

Fig. 7: Phase response as a function of the natural frequency Ω.

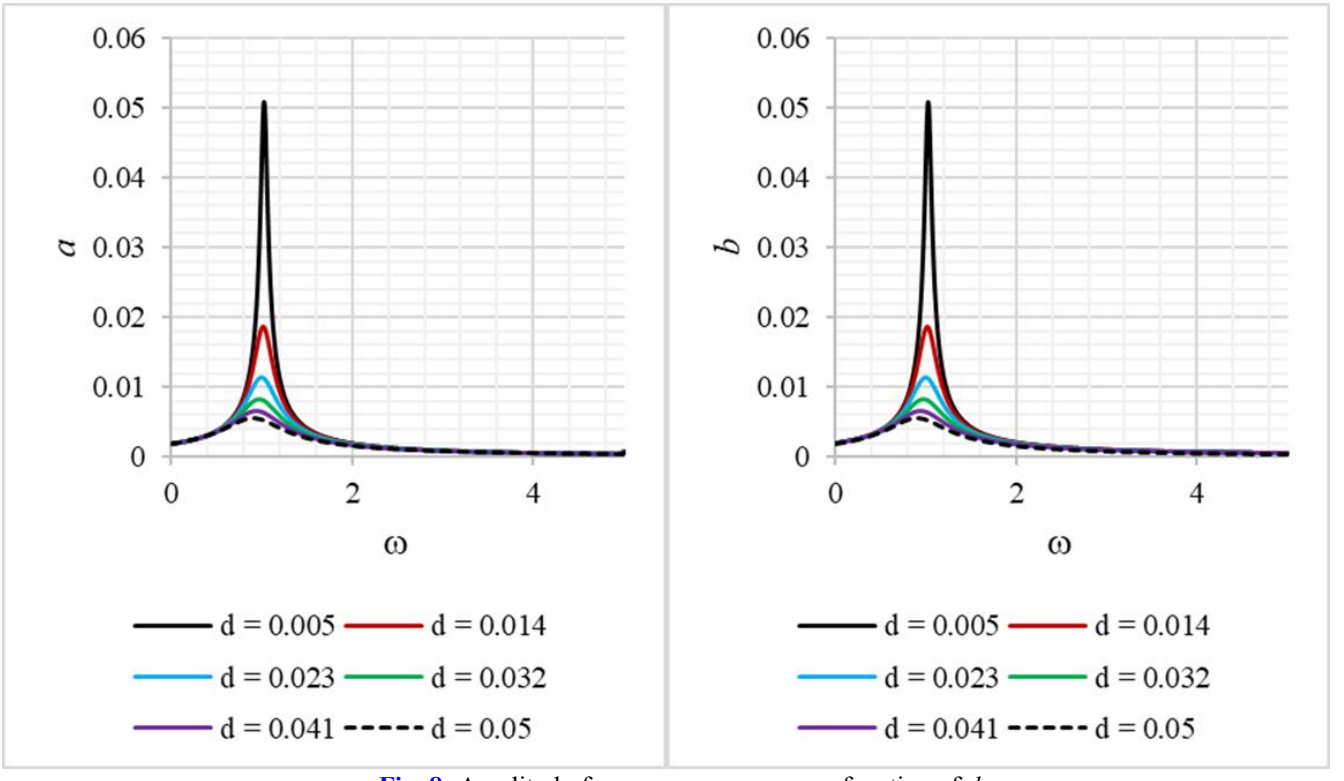

Fig. 8: Amplitude-frequency response as a function of *d*.

In general, with an increase in the value of the natural frequency Ω, it can be seen that the amplitude values of the main resonance decrease (almost exponentially, see Table 1, Figs. 6 and 7). The presented graphs show the behavior of the amplitude and phase-frequency characteristics of the system with a change in the natural frequency Ω. The frequency response (Fig. 6) demonstrates that as Ω increases, the resonance peak shifts to the right – to higher values of the angular velocity ω. At the same time, the height of the amplitude peak decreases sharply, and at Ω = 2.5 it becomes more than 5 times lower than at Ω = 0.5. This indicates the manifestation of the self-centering effect, *i.e.* the higher the rigidity of the system, the less the rotor deviates from the equilibrium position during excitation. Thus, an increase in the natural frequency leads to a decrease in the amplitude of vibrations even at resonance, which is critically important for increasing the stability of systems with active magnetic suspension.

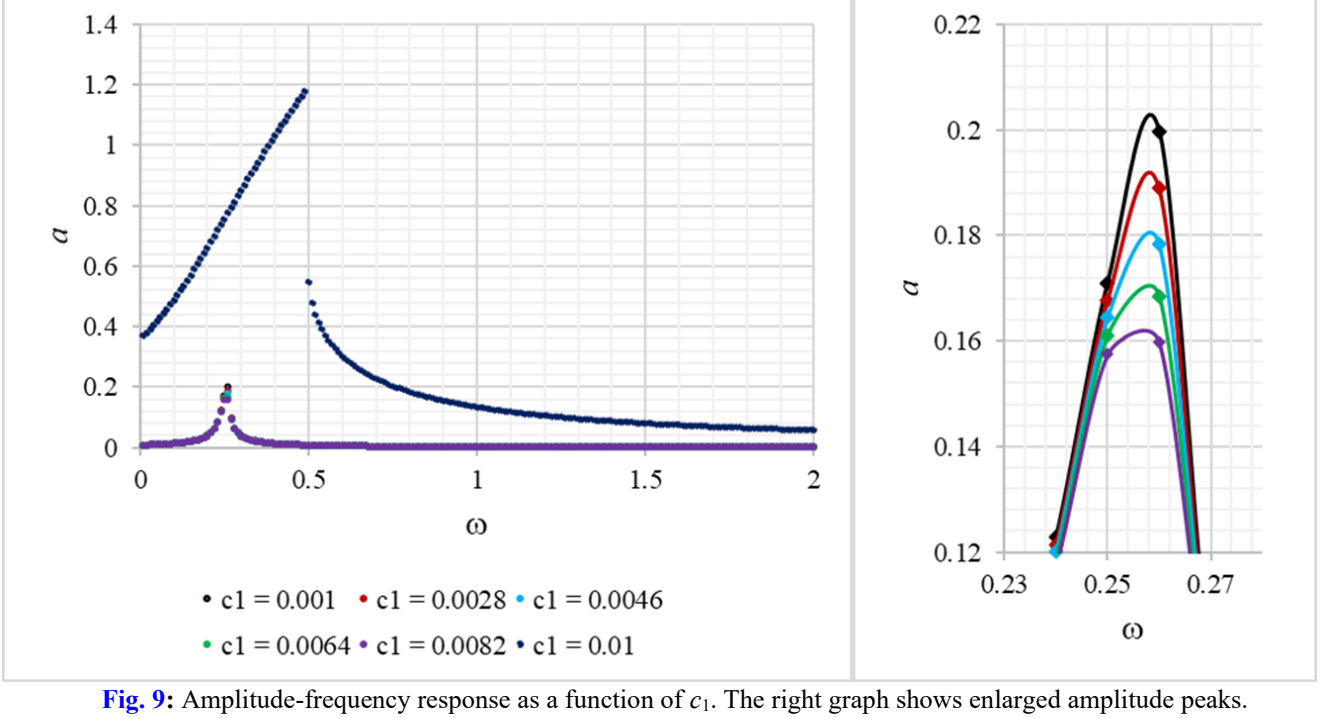

Fig. 9: Amplitude-frequency response as a function of c_1. The right graph shows enlarged amplitude peaks.

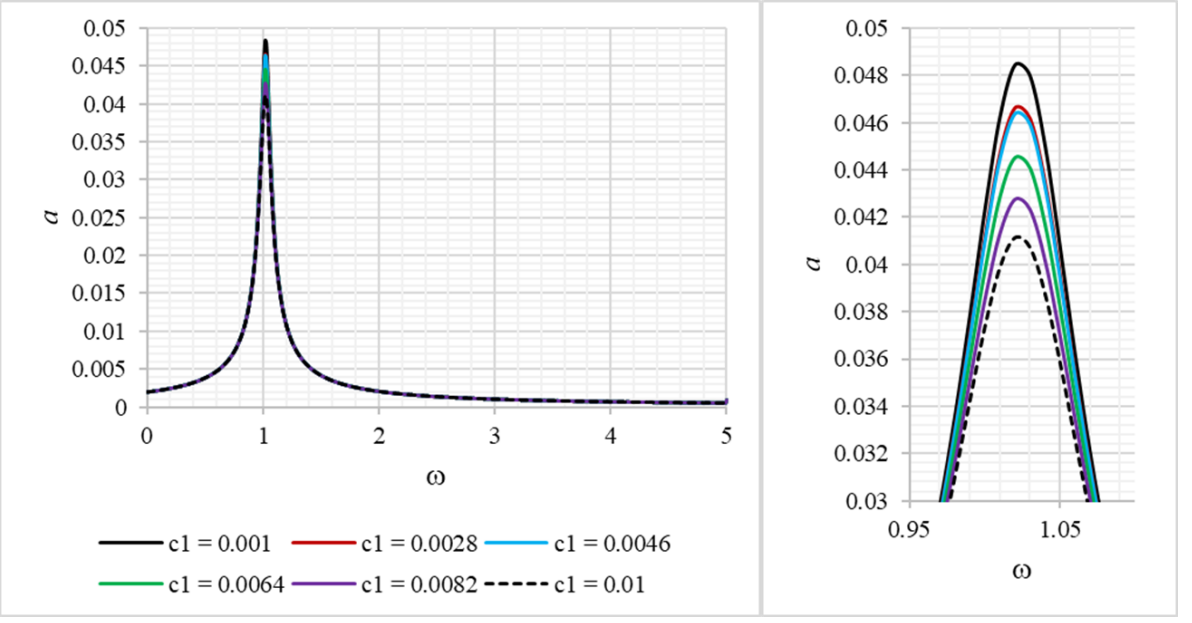

Fig. 10: Amplitude-frequency response as a function of c_1. The right graph shows enlarged amplitude peaks.

The phase-frequency characteristic (Fig. 7) shows that at each Ω, a typical phase jump occurs, passing from approximately -π/2 to +π/2 near the resonant frequency. With an increase in the natural frequency, this transition shifts to the right and becomes more compressed, *i.e.* the system switches phase more quickly when crossing the resonant frequency. This indicates an increase in the reactivity of the system, but at the same time, the phase sensitivity to disturbances decreases.

Thus, an increase in the natural frequency of the system not only reduces the amplitude of the resonant vibrations, but also stabilizes the phase response, making the system behavior more predictable and stable. This confirms the importance of a high natural frequency when designing systems with rotary motion, especially in the context of magnetic bearings, where stability and minimal vibration are critical.

The amplitude-frequency characteristics obtained from Eq. (27), *i.e.* when the shaft center performs an elliptical precessional motion about the equilibrium position, are shown in Figs. 8-13. With variation of *d*, the components of the amplitude of the elliptical precessional motion change similarly (Fig. 8).

In both cases, an increase in the parameter *d* leads to damping of forced vibrations of the system. For example, an increase in this parameter by an order of magnitude reduces the amplitude value ninefold.

In addition, with an increase in this value, a shift in the

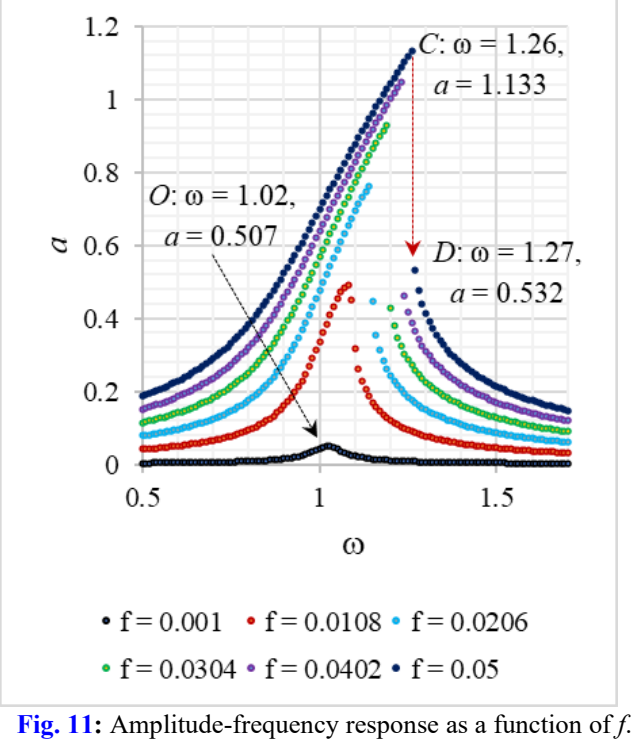

Fig. 11: Amplitude-frequency response as a function of *f*.

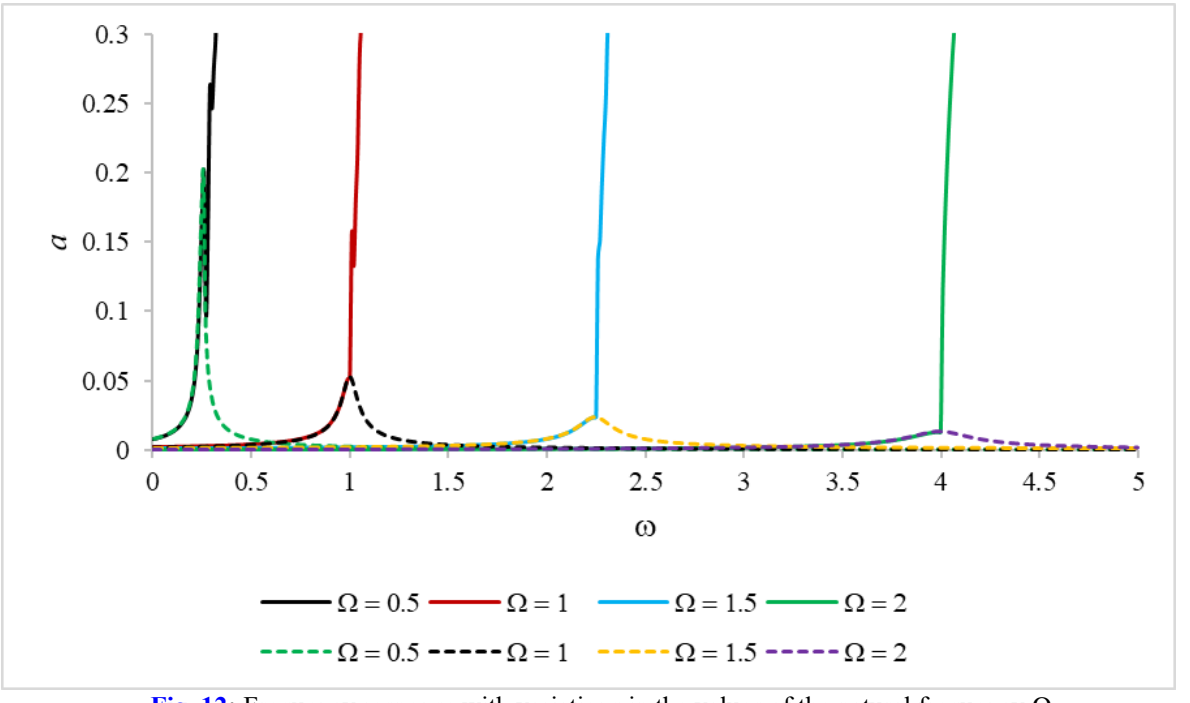

Fig. 12: Frequency response with variations in the values of the natural frequency Ω.

amplitude peak is observed towards a decrease in the natural frequency value from 1.02 to 0.9, which is also caused by the nonlinearity of the system.

With variation in c_1, the rotor amplitudes behave ambiguously (Figs. 9 and 10). For example, for the case of small values of the natural frequency of the rotor system (Ω < 1), an increase in the parameter c_1 by an order of magnitude leads to a shift in the resonance frequency (from ω = 0.26 to ω = 0.49) and to a sharp increase (by a factor of 5.86) and a breakdown of the vibration amplitudes, which is typical of systems with hard-type nonlinearity. Here, the breakdown of the amplitudes occurs at a frequency of ω = 0.49, increasing to a value of 1.179 (Fig. 9, point A), and then sharply decreases to 0.545 (Fig. 9, point B), maintaining a monotonically decreasing character. In the case of large values of the natural frequency of the gas centrifuge (Ω ≥ 1), the variation in the parameter c_1 does not generally have a strong effect on the dynamics of the system as a whole. For example, its increase by an order of magnitude dampens the vibrations insignificantly, reducing the amplitude values from 0.0484 to 0.0411 (Fig. 10), *i.e.* only 1.17-fold.

A more interesting picture is observed when varying the

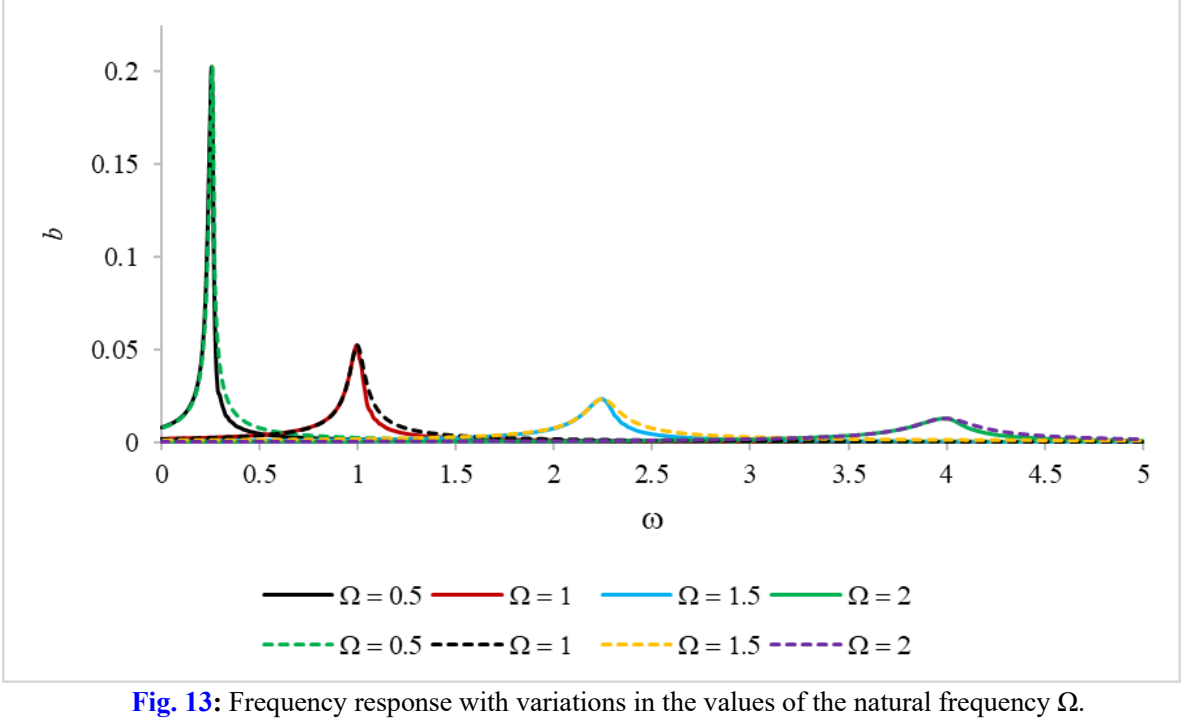

Fig. 13: Frequency response with variations in the values of the natural frequency Ω.

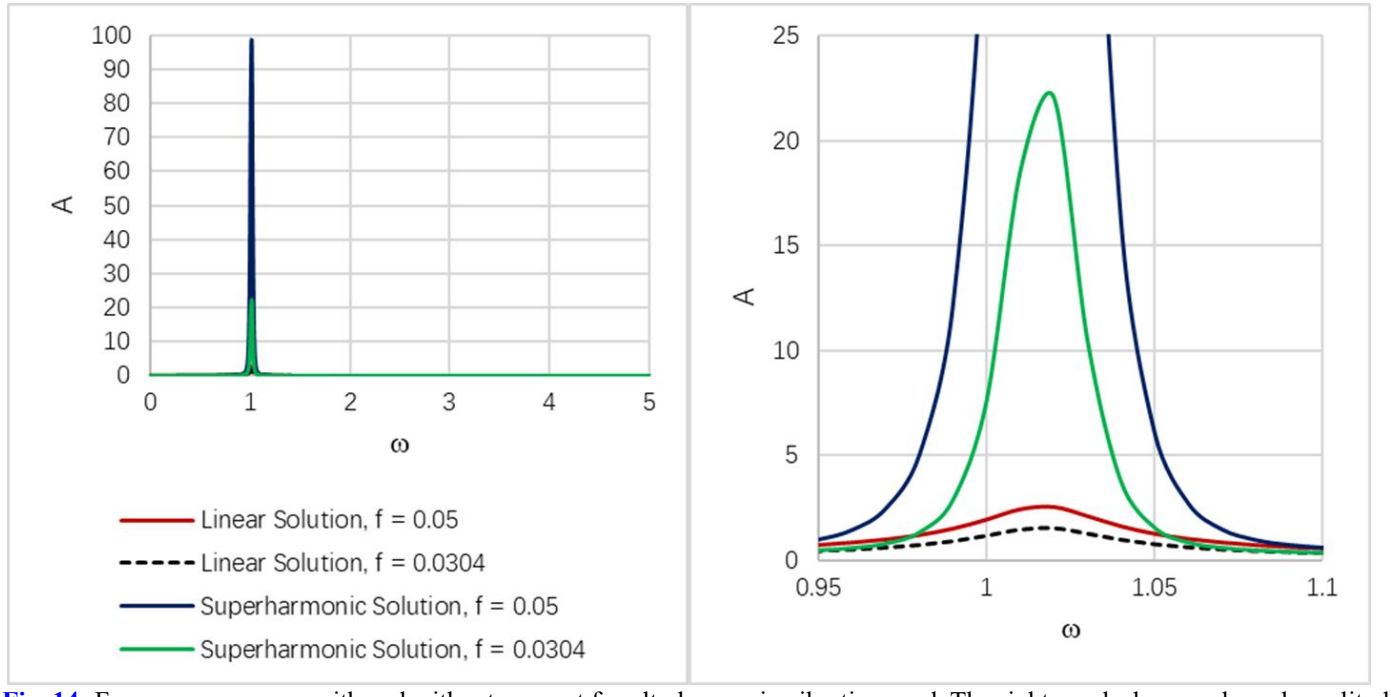

Fig. 14: Frequency response with and without account for ultraharmonic vibrations and. The right graph shows enlarged amplitude peaks.

parameter of the disturbing force – *f*, which generally characterizes the displacement of the rotor's center of inertia from its geometric center. Thus, an increase in this parameter by at least one order of magnitude leads to a proportional 9.6-fold increase in the amplitude of forced vibrations. Moreover, in this case, a shift in the resonance frequency from ω = 1.02 to ω = 1.08 and a breakdown of the amplitudes are observed. With a further increase in this parameter, the nonlinear features of the system are increasingly more expressed. For example, a 50-fold increase in *f* leads to a 22.35-fold increase in the amplitude of forced vibrations, whereas a shift in the resonance frequency and a breakdown of the amplitudes are already observed at ω = 1.26 (Fig. 11, point C).

To study the dynamics of amplitudes in the case of elliptical

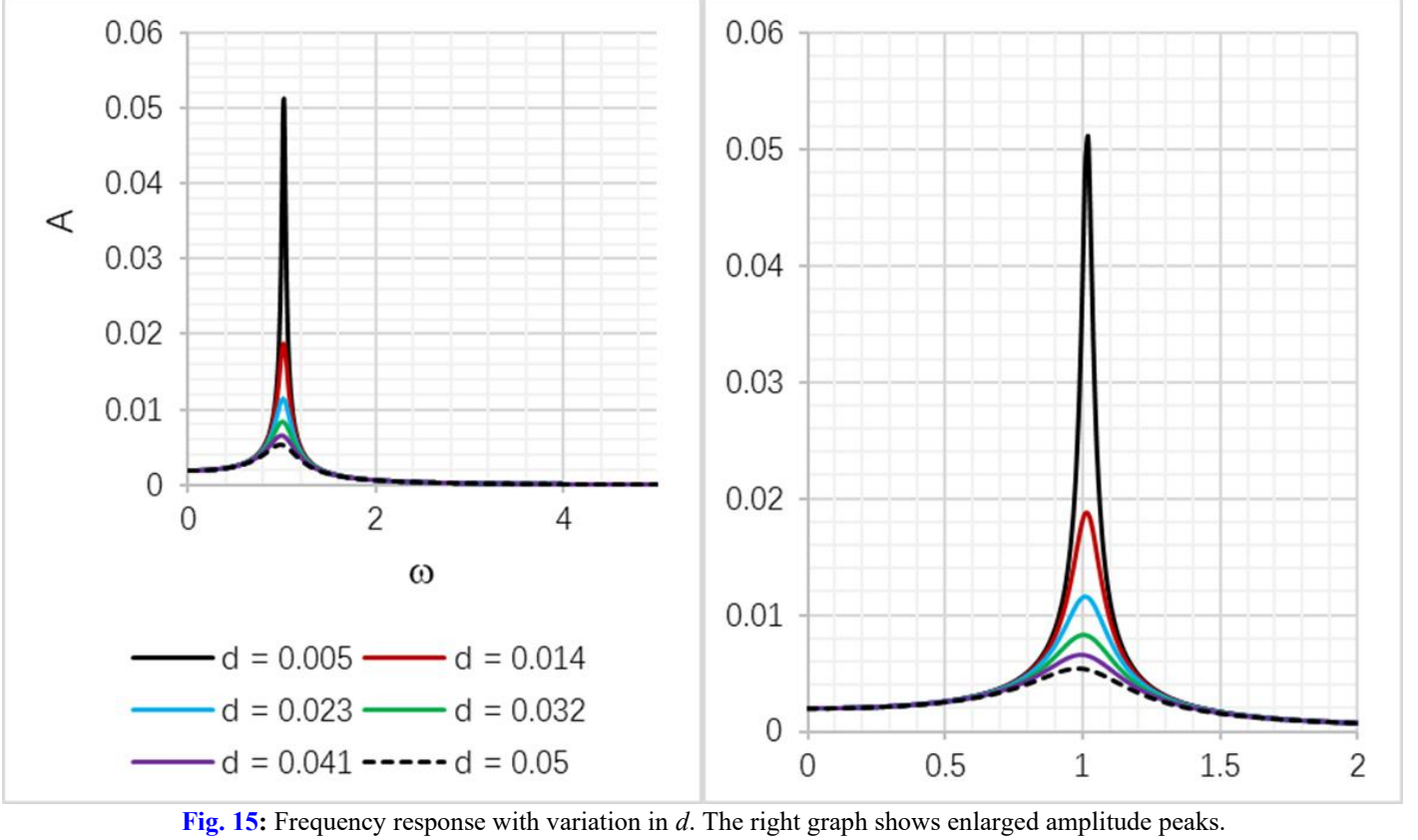

Fig. 15: Frequency response with variation in *d*. The right graph shows enlarged amplitude peaks.

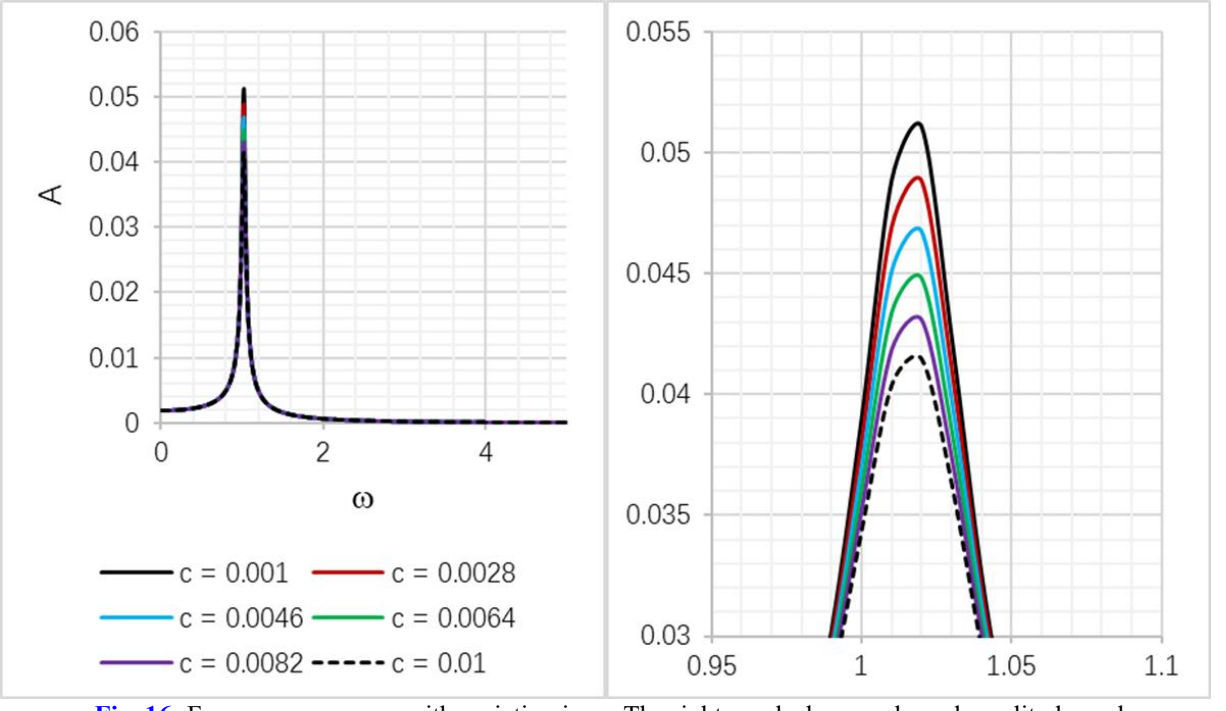

Fig. 16: Frequency response with variation in c_1. The right graph shows enlarged amplitude peaks.

precessional motion depending on the natural frequency, the amplitude-frequency characteristics of the components of elliptical motion *a* and *b* were constructed using analytical (Fig. 12, dotted curve) and numerical Runge-Kutta-Felberg methods of the 4th-5th order with an adaptive integration step, which allows us to change the integration step length based on the local error estimate, which in turn makes the method more efficient by reducing the step in areas with high curvature and increasing it in areas with low curvature, ensuring the uniform error distribution and saving computing resources (Fig. 12, solid curve). As can be seen in the case of the amplitude component *a*, the Runge-Kutta-Felberg numerical method for solving the differential equations of motion (7) does not give any significant results, tending to infinity after a certain value, which is caused by the bottleneck in the algorithm itself, as it contains division by zero, which cannot be included in the analytical method. For the case of the amplitude component *b*, the results of the numerical and analytical methods for solving the equations practically coincide (Fig. 13, solid curve). With an increase in the angular velocity of the rotor, the amplitudes of the main resonance decrease, which, as it was mentioned before, is associated with the self-centering effect characteristic of rotors in elastic supports.

The amplitude-frequency characteristics obtained from

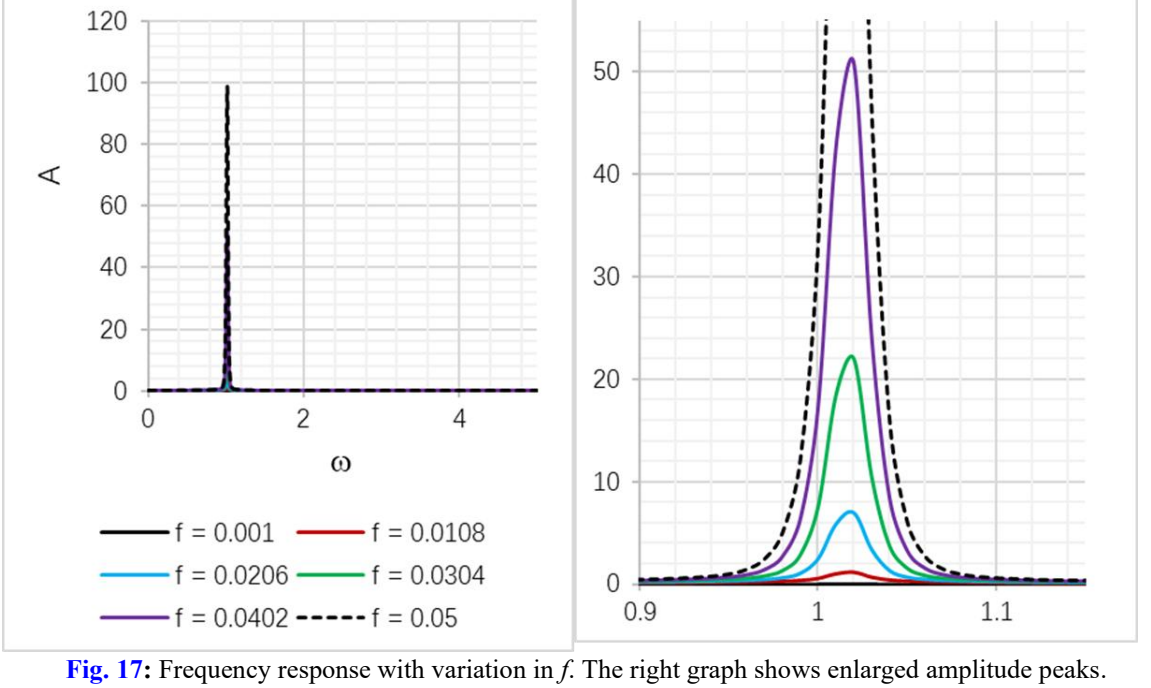

Fig. 17: Frequency response with variation in *f*. The right graph shows enlarged amplitude peaks.

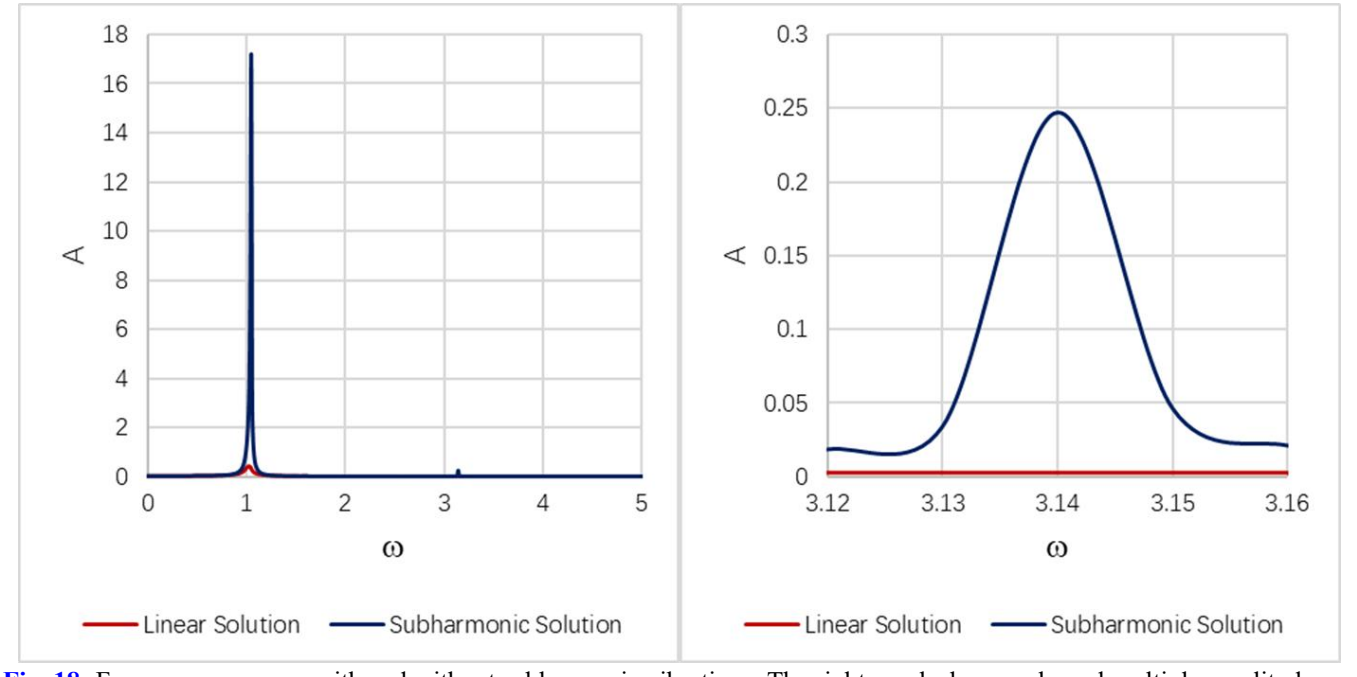

Fig. 18: Frequency response with and without subharmonic vibrations. The right graph shows enlarged multiple amplitude peaks.

Eq. (43) for ultraharmonic (or superharmonic) vibrations are shown in Figs. 14-17. It can be seen that ultraharmonic vibrations make a significant contribution to the main resonance of the system, increasing it by several orders of magnitude. This contribution becomes more pronounced with an increase in the parameter f, which characterizes the displacement of the rotor's center of inertia due to various errors that occur during production, which subsequently necessitate balancing of rotor systems. In this case, the appearance of additional resonances in the system is not observed. For example, if we increase this parameter by a factor of one and a half (from $f = 0.0304$ to $f = 0.05$) without taking into account ultraharmonic vibrations, the amplitudes of the gas centrifuge will also proportionally increase by almost one and a half (Fig. 14, solid red and dotted black curves). Then, when taking into account superharmonic vibrations, the main resonance increases 14-fold for $f = 0.0304$ (Fig. 14, solid green curve), and 38-fold for $f = 0.05$ (Fig. 14, solid blue curve), which already determines the necessity of accounting for this type of vibrations when designing rotor systems and calculating their strength.

When varying the parameter d, the dynamics of the system

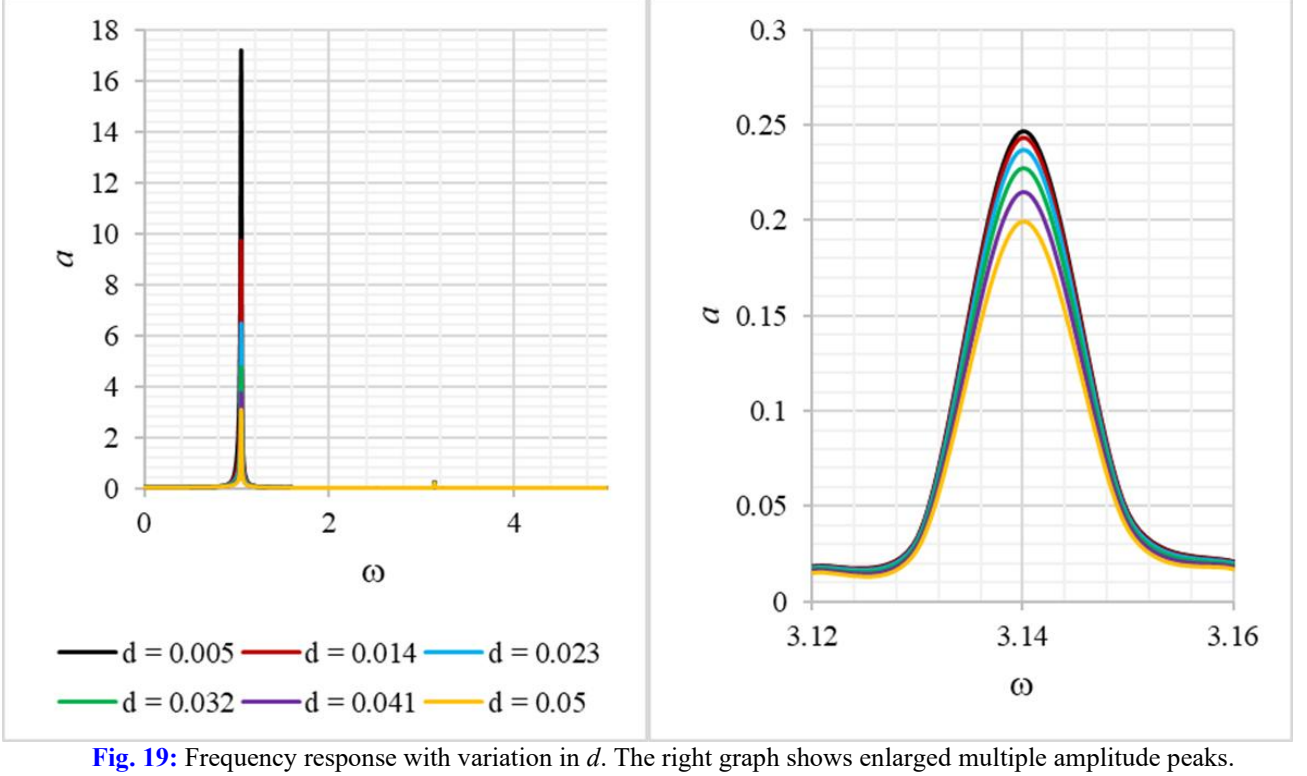

Fig. 19: Frequency response with variation in d. The right graph shows enlarged multiple amplitude peaks.

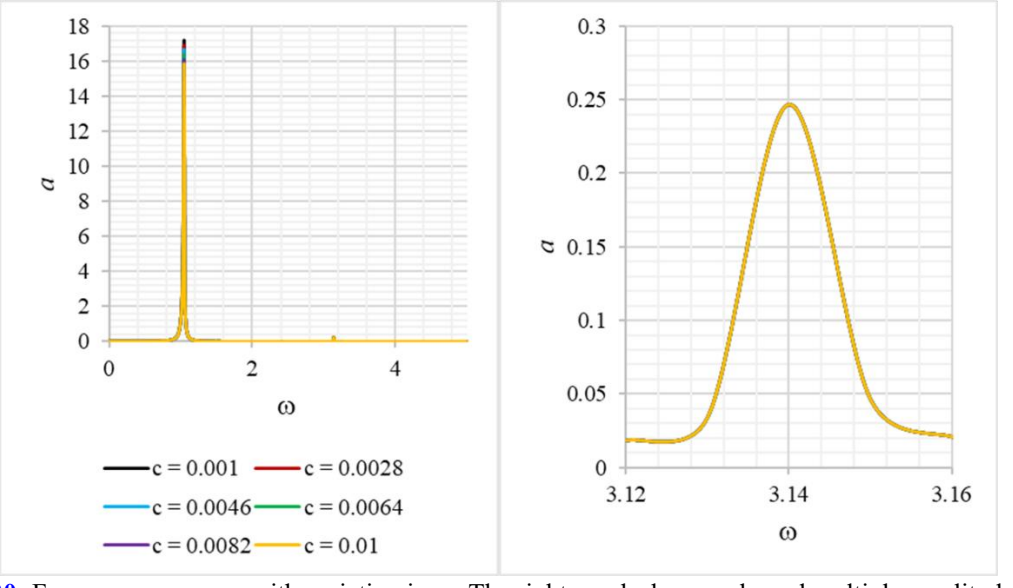

Fig. 20: Frequency response with variation in c_1. The right graph shows enlarged multiple amplitude peaks.

with account for ultraharmonic vibrations is similar to the previous cases (Fig. 15). A gradual increase in this parameter leads to a gradual decrease in the amplitude value, whereas the shift of the main resonant frequency is not observed. For example, when d increases 3-fold, the amplitude also decreases 3-fold (Fig. 15, red solid curve). It should be noted that this pattern is practically preserved, and when d increases 4.6-fold, it leads to a 4.4-fold decrease in the amplitude (Fig. 15, blue solid curve). Then the intensity of amplitude damping decreases and already when the parameter d increases by an order of magnitude, the amplitude decreases only 1.2-fold compared to the previous case (Fig. 15, black dotted curve).

As before, variations in the parameter c_1 do not markedly affect the dynamics of the system, the exception is the case of small values of the natural frequency of the rotor system ($\Omega < 1$). Thus, we can conclude that an increase in the value of the natural frequency damps the effects of nonlinearity and linearizes the system (Figs. 9 and 16). Whereas in the case of $\Omega \geq 1$, an increase in the parameter c_1, as before, leads to an insignificant (within 15%) decrease in the amplitude values. No shift in the main resonance frequency is observed when c_1 is varied.

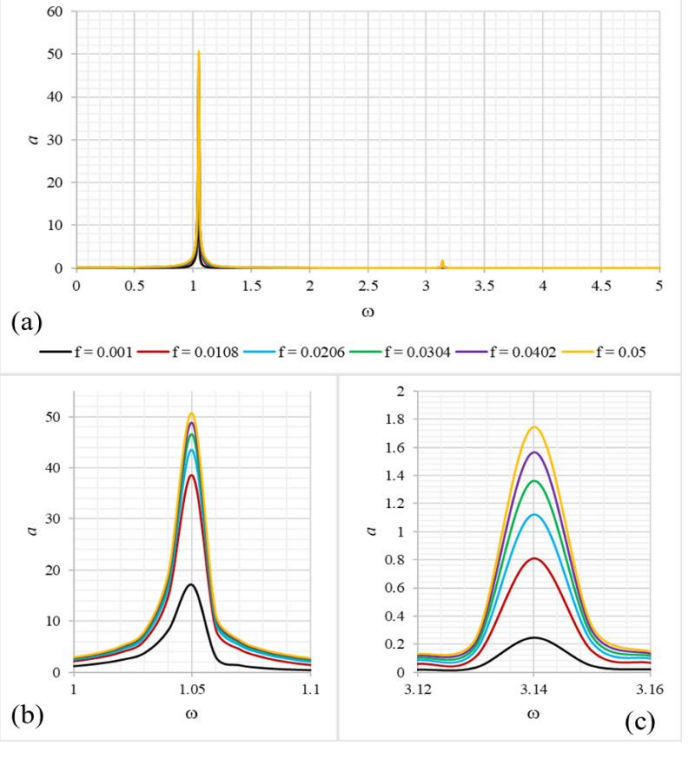

Fig. 21: Frequency response with f variation. Case a) Amplitude peaks over the entire modeling interval. Case b) Enlarged amplitude peaks of the main resonance. Case c) Enlarged amplitude peaks of the multiple resonance.

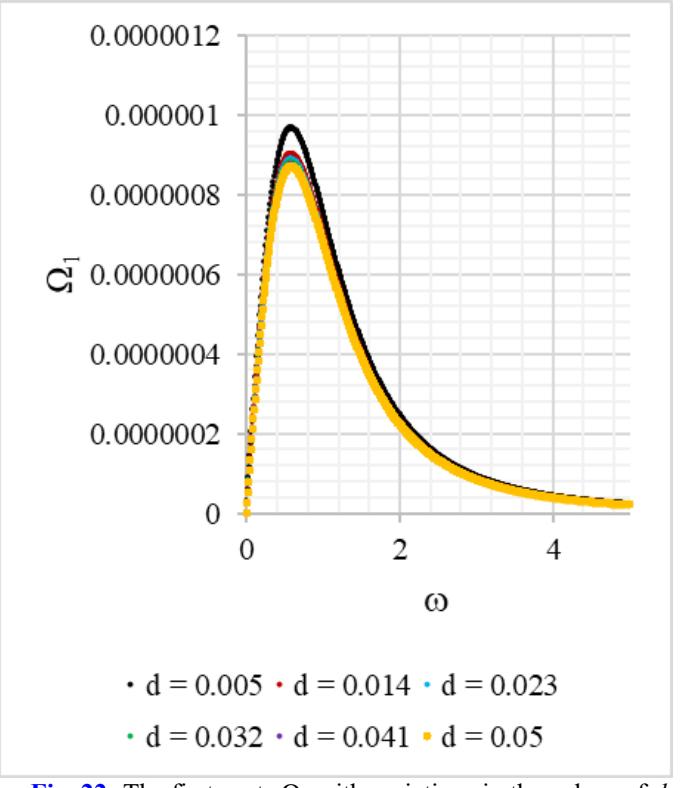

Fig. 22: The first roots Ω_1 with variations in the values of d.

As it was mentioned above, the variation of f has a rather strong effect on the amplitude values of the system when ultra harmonic vibrations are taken into account. For example, an increase in this parameter by almost 11 times (from 0.001 to 0.0108) leads to a proportional increase in the amplitude by 22 times (Fig. 17, red solid curve). Accordingly, a further 2-fold increase in f leads to a 6-fold increase in the amplitude of the gas centrifuge (Fig. 17, blue solid curve). Another 1.5-fold increase in f, gives an almost 3-fold increase in the amplitude (Fig. 17, green solid curve). Thus, increasing f to 0.05 (*i.e.* 50 times) we can observe an increase in the amplitude to 97.74, *i.e.* almost 2000 times, which shows that account for ultra harmonic vibrations is critically important for (hard-type) systems with (cubic) nonlinearity.

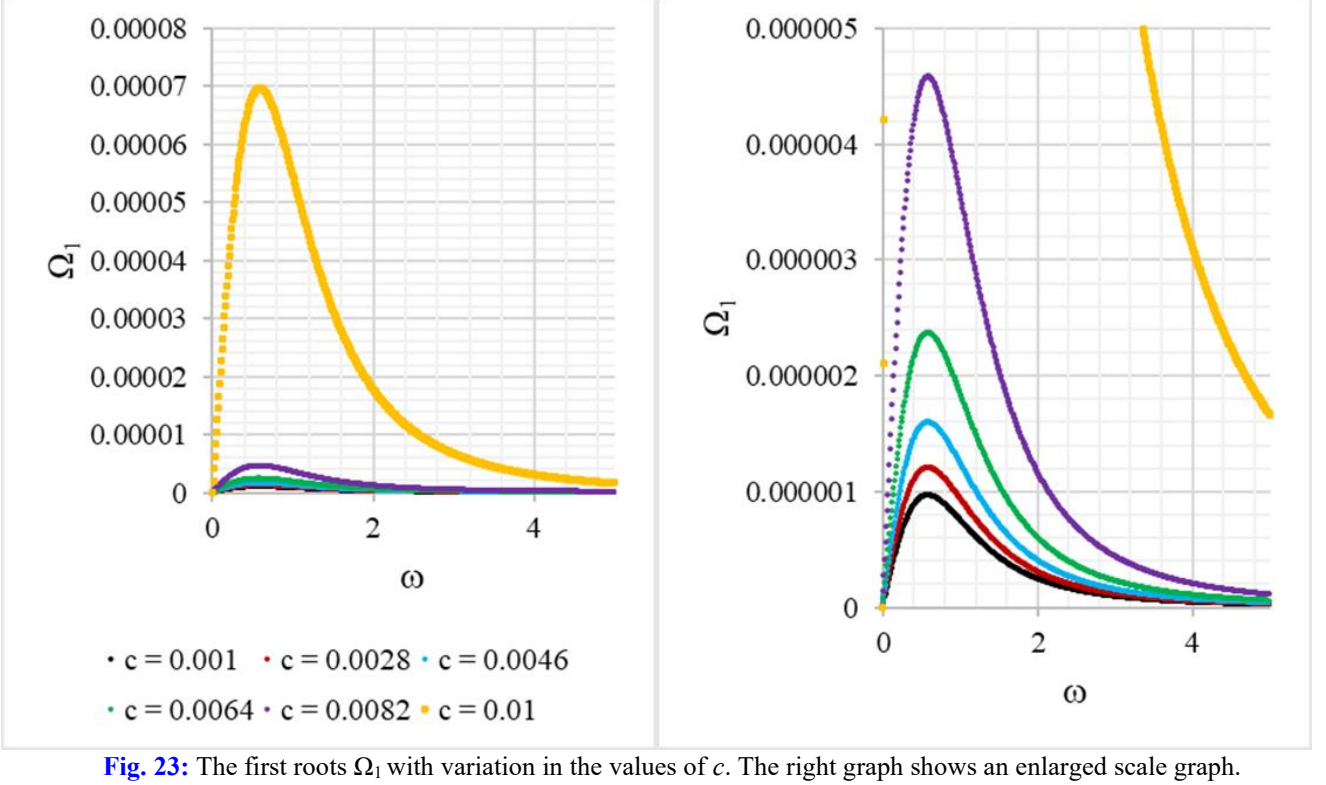

Fig. 23: The first roots Ω_1 with variation in the values of c. The right graph shows an enlarged scale graph.

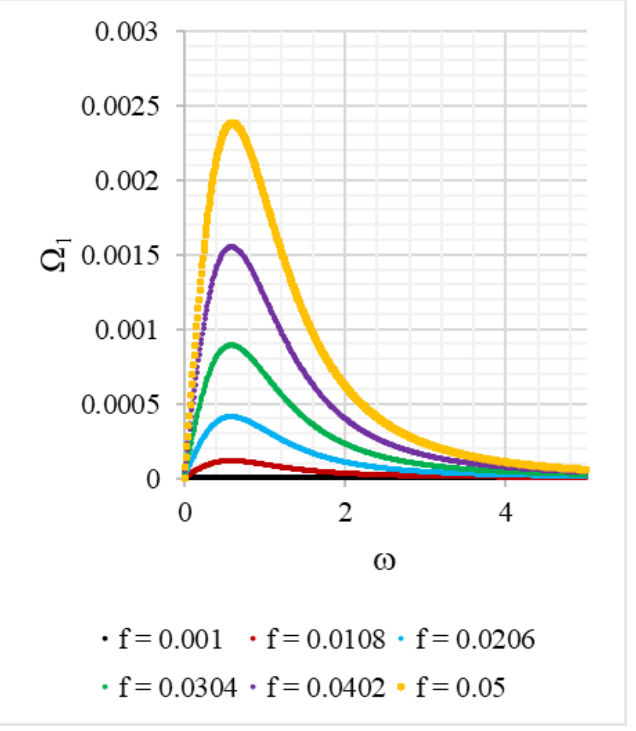

Fig. 24: The first roots $\Omega_1$with variation in the values of *f*.

No less interesting is the case of subharmonic vibrations. As Fig. 18 shows, when subharmonic vibrations are into account, several resonances are superimposed on the rotor system. The first superposition occurs at the main resonance, and a significant increase in the amplitude is observed for the first resonance (Fig. 18, the left figure, blue solid curve). The second superposition occurs at a frequency multiple of the system nonlinearity, namely at 3Ω, which is typical of the systems described by the Duffing equation (Fig. 18, the right figure, blue solid curve). Thus, the appearance of additional resonance regions should be taken into account when choosing operating frequencies and modes, which is especially important for high-speed rotor systems.

An increase in the parameter *d*, as before, strongly dampens the vibrations of the rotor system (see Fig. 19). However, damping of the amplitudes is clearly expressed only at the main resonance; the resonance at 3Ω is not so sensitive to variations in this parameter. For example, with an increase in *d* by an order of magnitude, the amplitude at the main resonance decreases by 5.5 times, while damping at 3Ω is only 1.25 times (Fig. 19, black and yellow solid curves).

As before, the variation in c_1 has virtually no effect on the

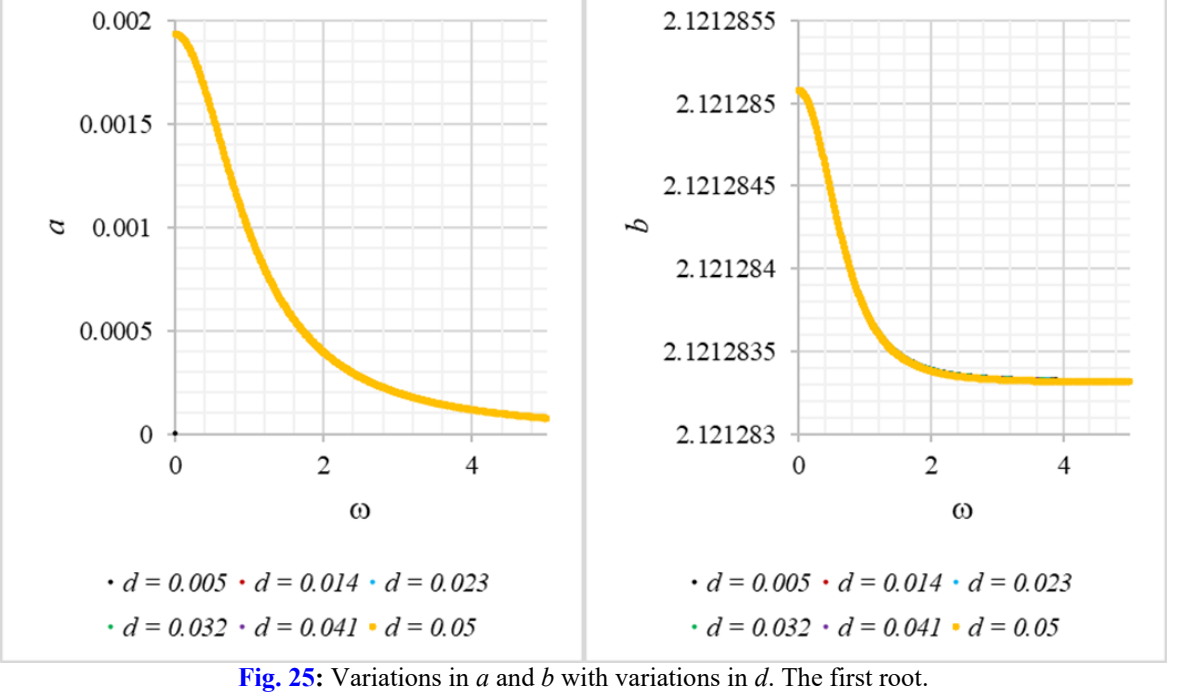

Fig. 25: Variations in *a* and *b* with variations in *d*. The first root.

Table 1: Amplitudes of the main resonance.

ω_0	0.52	1.1	1.5	2.0
A_i	0.46	0.42	0.34	0.28
$q = A_{i+1}/A_i$ – ratio of amplitudes, i = 1...5.	1	0.90	0.82	0.81

resonances of the system (Fig. 20). In the case of the main resonance, with a 10-fold increase in this parameter (from c_1 = 0.001 to c_1 = 0.01), only a 7.8-fold decrease in the amplitude is observed (Fig. 20, the left figure, black and yellow solid curves, respectively), whereas at a frequency multiple of the main critical speed of 3Ω, damping is not observed at all (Fig. 20, the right figure).

An increase in f in the case of subharmonic vibrations causes an equal increase in the amplitude both of the main and of the multiple resonance of the rotor system (Fig. 21, case a). It is worth noting that an increase in this parameter does not lead to a proportional increase in both resonances. For example, if f increases from 0.001 to 0.0108, the amplitude of the main resonance increases 2.25-fold (Fig. 21, case b), and that of the multiple resonance 3.3-fold (Fig. 21, case c), whereas an increase in f from 0.0402 to 0.05 leads to an increase in the amplitudes 1.04-fold and 1.11-fold, respectively. No displacement of the amplitudes or their breakdown is observed.

In the case of self-excited vibrations, the lowest frequency of the system, *i.e.* the first root of Eq. (60), and the corresponding amplitudes are also quite sensitive to the above parameters (Figs. 22-24). For example, an increase in c_1 and f leads to an increase in the frequency of self-excited vibrations of the system (Fig. 23 and 24). When c_1 changes from 0.001 to 0.0082 the frequencies of self-excited vibrations increase uniformly (Fig. 23, red, blue, green and purple solid curve), however, at c_1= 0.001 we can observe a sharp increase in the frequency of the rotor system (Fig. 23, yellow solid curve) In case of f variation, the growth in self-excited variation frequencies of the gas centrifuge is smoother and more uniform. For example, a smooth increase in f from 0.001 to 0.0108 leads to a shift in the frequency values from $9.667 \cdot 10^{-7}$ to 0.0001126. Further increase in f from 0.0108 to 0.0206, gives an increase in frequency to 0.00041, *i.e.* 4-fold. Thus, continuing to increase the value of f to 0.05, we notice a shift in the self-excited variation frequency to 0.0024.

As for the amplitudes of self-excited vibrations, changes in d and c_1 parameters do not affect them in any way (Fig. 22). For example, a change in these parameters within one order of magnitude (for d: from 0.005 to 0.05, for c_1: from 0.001 to 0.01) demonstrates a weak impact on the amplitudes of the self-excited vibrations of the system. The amplitudes of the system vibrations a and b have maximum values at the beginning of the process and then rapidly decrease. The amplitude b reaches its minimum value at ω = 2.5 and then practically retains its value (Figs. 25 and 26), which is typical of the case of self-excited variations. Variations in the parameter f have a rather strong effect on the dynamics of the gas centrifuge (Fig. 27). The graphs show the dependences of the amplitudes a and b on the frequency ω for different values of the parameter f. In both cases, with an increase in f, the initial amplitudes increase and reach a maximum at small values of ω, after which they decrease exponentially. For the amplitude a (Fig. 27, the left figure), the decrease is more pronounced: at large f values, the amplitude first increases sharply, and then quickly fades to zero. The amplitude b (Fig. 27, the right figure) is characterized by similar behavior, but its decrease is less sharp, and it does not fade completely, but tends to a certain constant value.

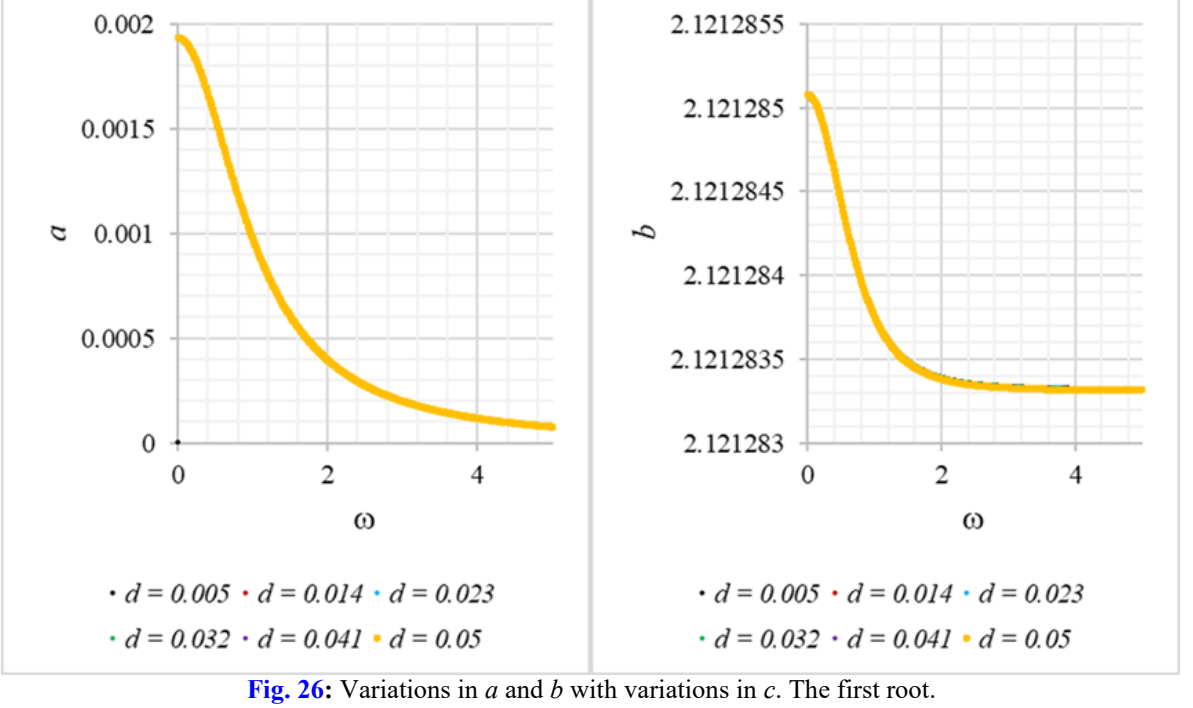

Fig. 26: Variations in a and b with variations in c. The first root.

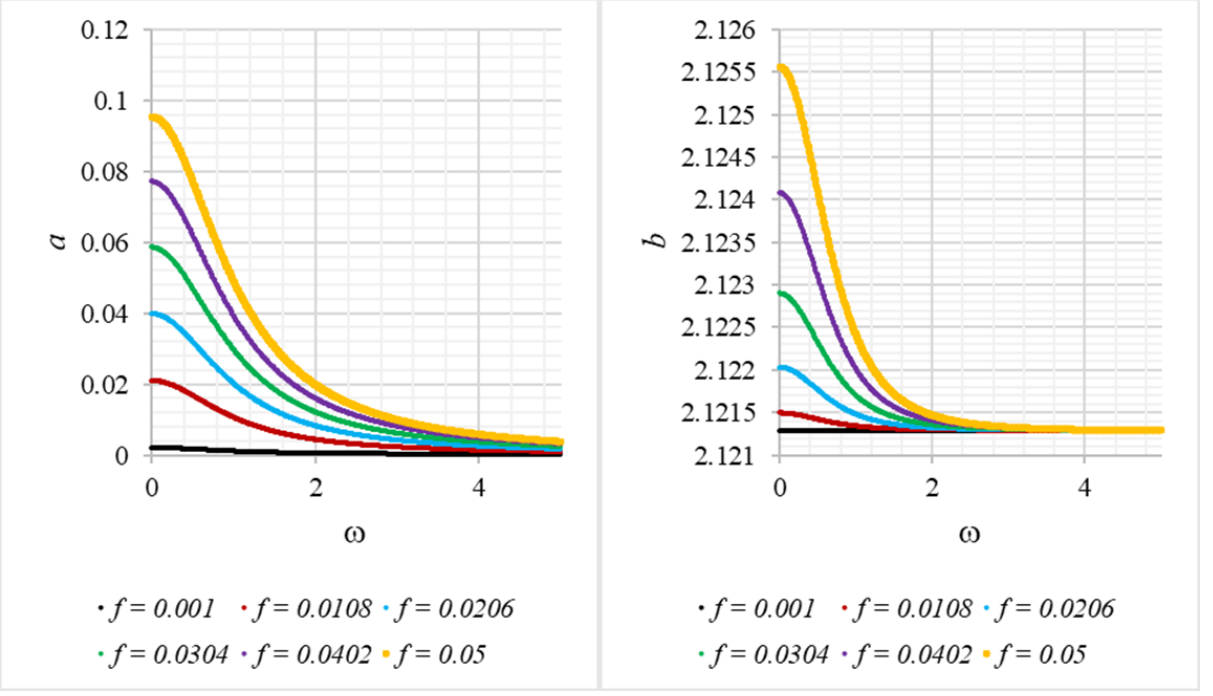

Fig. 27: Variations in *a* and *b* with variations in *f*. The first root.

4. Conclusion

In this paper analytical solutions and amplitude-phase frequency characteristics were obtained for the cases of natural, forced and self-excited vibrations of the system for both circular and elliptical precessional motion. The cases of ultra- and subharmonic vibrations typical of nonlinear systems were studied. This research allowed us to analyze in detail the influence of parameters d, c_1 and f on the amplitude-phase frequency characteristics of the system described by a cubic equation. As a result, it was found that with an increase in the parameter d, a significant damping of the resonant amplitudes is observed, which is confirmed by the shift and decrease in the amplitude peaks for both circular and elliptical precessional motion. This phenomenon is explained by an increase in the viscous resistance of the system, which leads to a decrease in the intensity of oscillatory processes and a faster attenuation of self-excited vibrations. The parameter c_1 demonstrated a weak effect on the dynamics of amplitudes, which indicates its secondary role in the formation of self-excited vibrations for the natural frequencies of the system at $\Omega > 1$. Otherwise, a change in this parameter would lead to the predominance of nonlinear effects such as amplitude breakdown for the elliptical precessional motion in the system. This allows us to conclude that regulation of this parameter does not have a significant effect on the overall dynamics of the system and can be used for fine adjustment of vibration characteristics. An increase in the parameter f leads to an increase in the size of the elliptical orbit – the amplitudes of vibrations along the major and minor axes of the ellipse will increase almost proportionally to the magnitude of the imbalance. With a sufficiently large f, one can expect a manifestation of the rigid nonlinearity effects – the appearance of a shift in resonance peaks and nonlinear effects similar to the circular case. In the case of ultra- and subharmonic vibrations, there is a significant increase in the amplitudes at the main resonance and imposition of an additional resonance at 3Ω, which shows the importance of their consideration in designing similar rotor systems. In the case of ultra harmonic vibrations, the main frequency of vibrations is "fed" by nonlinear effects, which sharply increases their amplitude. In fact, this is an analogue of internal resonances: although the external effect has a single frequency (the rotor rotation frequency), the nonlinear force generates multiple frequencies that can resonate with the natural frequency of the system. Additional resonant frequencies do not appear; however, the main oscillation mode grows. Such a nonlinear resonance is especially actively pronounced in the conditions of a large imbalance and high stiffness of the system (cubic elastic characteristic), and its limitation requires either a decrease in nonlinearity (for example, work with smaller amplitudes, balancing of the rotor) or active control. The emergence of a resonance at a frequency of 3ω under the action of an impact force rotating with a frequency ω is a typical manifestation of a subharmonic resonance in the nonlinear system. Cubic nonlinearity allows the system to fluctuate with a period greater than the period of the external action. This additional fluctuation does not arise in the linear system, but it may arise in the presence of nonlinearity, as part of the excitation energy is transmitted in the fluctuation at a triple frequency. The absence of the amplitude breakdown indicates that this resonance develops according to a "soft" scenario – the system smoothly enters a new mode without bifurcations such as the amplitude breakdown. At the same time, the parameter f has a noticeable effect on the frequency characteristics of the system, determining both stability and the form of self-excited vibrations. With an increase in f, the initial amplitude of self-

excited vibrations increases, however, the rate of their attenuation also increases. It is important to note that the amplitude of self-excited vibrations does not completely attenuate, but tends to a certain constant value, indicating the presence of a stable vibration mode for some system parameters. This phenomenon indicates the possibility of existence of stationary self-excited vibrations that persist under constant external impact. The shift of the center of inertia of the system has almost no effect on the established amplitude of self-excited vibrations – it is determined by the internal nonlinear dynamics. The presence of a small impact force, although it shifts the equilibrium point, does not significantly change the limit cycle. In general, an increase in the value of the natural frequency reduces the value of the amplitudes due to the self-centering effect for all types of precessional motion, but it should be taken into account that even for the case of elliptical motion, the use of numerical methods does not give sufficiently accurate results. Thus, the obtained results confirm the adequacy of the developed model and its applicability for predicting the behavior of oscillatory systems in various operating modes. In practical terms, this means that the use of the proposed approach allows more accurate control of the amplitudes and phases of vibrations, which can find application in various technical devices, including vibration diagnostics and active damping systems. Further, this study can be expanded to analyze more complex nonlinear systems taking into account additional parameters, such as nonlinear resistance and the presence of random disturbances. This will allow specialisrs to create more universal models capable of taking into account a wide range of external and internal factors affecting the dynamics of self-excited vibrations. As a result of further development of the proposed methodology, new data on the behavior of systems under resonant and non-resonant conditions can be obtained, which will open up opportunities for creating more effective algorithms for controlling dynamic systems.

Acknowledgments

This work was supported by the research project (AP19677384 - Development and research of the dynamics of a gas centrifuge on magnetic bearings with nonlinear characteristics and a control system) of the Ministry of Education and Science of the Republic of Kazakhstan and was performed at Research Institute of Mathematics and Mechanics in Al-Farabi Kazakh National University.

Conflict of Interest

There is no conflict of interest.

Supporting Information

Not applicable.

CRediT Statement

Almatbek Kydyrbekuly, **Rakhmetolla A.Sh.:** Methodology. **Almatbek Kydyrbekuly**, **Rakhmetolla A.Sh.**, **Gulama-Garip Alisher E. Ibrayev:** Formal analysis. **Almatbek Kydyrbekuly**, **Rakhmetolla A.Sh.**, **Gulama-Garip Alisher E. Ibrayev:** Software. **Gulama-Garip Alisher E. Ibrayev**, **Shabdan E.:** Investigation. **Gulama-Garip Alisher E. Ibrayev**, **Shabdan E.:** Visualization. **Gulama-Garip Alisher E. Ibrayev:** Writing, original draft. **Almatbek Kydyrbekuly**, **Rakhmetolla A.Sh.**, **Gulama-Garip Alisher E. Ibrayev**, **Shabdan E.:** Writing, review & editing.

References

[1] G. Schweitzer, E.H. Maslen, H. Bleuler, Magnetic bearings, Theory, design and application to rotating machinery. Berlin: Springer, 2009.

[2] B. Polajzer, G. Tumberger, J. Ritonja, D. Dolinar, Linearization of radial force characteristic of active magnetic bearings using finite element method and differential evolution, *Magnetic Bearings, Theory and Applications*, Sciyo, 2010, doi: 10.5772/10086.

[3] H. Kim, H. C. Kim, Modeling and control of a magnetic bearing system for the magnetically suspended centrifugal blood pump, *The International Journal of Artificial Organs*, 2000, **23**, 689-696, doi: 10.1177/039139880002301006.

[4] M. N. Sahinkaya, A. E. Hartavi, C. R. Burrows, R. N. Tuncay, BIAS Current optimisation and fuzzy controllers for magnetic bearings in turbo molecular pumps, *Ninth International Symposium on Magnetic Bearings*, 2004.

[5] A. Chiba, T. Fukao, O. Ichikawa, Magnetic bearings and bearingless drives, Oxford: Elsevier Linacre House, 2005.

[6] J. C. Ji, C. H. Hansen, A. C. Zander, Nonlinear dynamics of magnetic bearing systems, *Journal of Intelligent Material Systems and Structures*, 2008, **19**, 1471-1491, doi: 10.1177/1045389x08088666.

[7] A. M. Mohamed, F. P. Emad, Nonlinear oscillations in magnetic bearing systems, *IEEE Transactions on Automatic Control*, 1993, **38**, 1242-1245, doi: 10.1109/9.233159.

[8] D. Laier, R. Markert, Simulation of nonlinear effects on magnetically suspended rotors, *First Conference on Engineering Computation and Computer Simulation ECCS-1*, 1995, **1**, 473-482.

[9] H. Springer, G. Schlager, T. Platter, Non-linear simulation model for active magnetic bearing actuators, *Sixth International Symposium on Magnetic Bearings*, 1998.

[10] N. Steinschaden, H. Springer, Some nonlinear effects of magnetic bearings, *17th Biennial Conference on Mechanical Vibration and Noise*, Las Vegas, Nevada, USA, American Society of Mechanical Engineers, September 12-16, 1999, 1753-1761, doi: 10.1115/detc99/vib-8063.

[11] J. C. Ji, L. Yu, A. Y. T. Leung, Bifurcation behavior of a rotor supported by active magnetic bearings, *Journal of Sound and Vibration*, 2000, **235**, 133-151, doi: 10.1006/jsvi.2000.2916.

[12] J. C. Ji, Dynamics of a piecewise linear system subjected to a saturation constraint, *Journal of Sound and Vibration*, 2004, **271**,

905-920, doi: 10.1016/S0022-460X(03)00759-4.
[13] J. C. Ji, C. H. Hansen, Analytical approximation of the primary resonance response of a periodically excited piecewise non-linear–linear oscillator, *Journal of Sound and Vibration*, 2004, **278**, 327-342, doi: 10.1016/j.jsv.2003.10.022.
[14] J. C. Ji, C. H. Hansen, Approximate solutions and chaotic motions of a piecewise nonlinear–linear oscillator, *Chaos, Solitons & Fractals*, 2004, **20**, 1121-1133, doi: 10.1016/j.chaos.2003.09.022.
[15] J. C. Ji, C. H. Hansen, On the approximate solution of a piecewise nonlinear oscillator under super-harmonic resonance, *Journal of Sound and Vibration*, 2005, **283**, 467-474, doi: 10.1016/j.jsv.2004.05.033.
[16] L. N. Virgin, T. F. Walsh, J. D. Knight, Nonlinear behavior of a magnetic bearing system, *Journal of Engineering for Gas Turbines and Power*, 1995, **117**, 582-588, doi: 10.1115/1.2814135.
[17] M. Chinta, A. B. Palazzolo, Stability and bifurcation of rotor motion in a magnetic bearing, *Journal of Sound and Vibration*, 1998, **214**, 793-803, doi: 10.1006/jsvi.1998.1549.
[18] J. C. Ji, A. Y. T. Leung, Non-linear behavior of a magnetically supported rotor, Seventh International Symposium on Magnetic Bearings, 2000.
[19] J. C. Ji, C. H. Hansen, Non-linear oscillations of a rotor in active magnetic bearings, *Journal of Sound and Vibration*, 2001, **240**, 599-612, doi: 10.1006/jsvi.2000.3257.
[20] J. C. Ji, A. Y. T. Leung, Non-linear oscillations of a rotor-magnetic bearing system under superharmonic resonance conditions, *International Journal of Non-Linear Mechanics*, 2003, **38**, 829-835, doi: 10.1016/S0020-7462(01)00136-6.
[21] J. C. Ji, Stability and Hopf bifurcation of a magnetic bearing system with time delays, *Journal of Sound and Vibration*, 2003, **259**, 845-856, doi: 10.1006/jsvi.2002.5125.
[22] J. C. Ji, C. H. Hansen, Non-linear oscillations of a rotor in active magnetic bearings, *Journal of Sound and Vibration*, 2001, **240**, 599-612, doi: 10.1006/jsvi.2000.3257.
[23] Y. S. Ho, H. Liu, L. Yu, Effect of thrust magnetic bearing on stability and bifurcation of a flexible rotor active magnetic bearing system, *Journal of Vibration and Acoustics*, 2003, **125**, 307-316, doi: 10.1115/1.1570448.
[24] W. Zhang, X. P. Zhan, Periodic and chaotic motions of a rotor-active magnetic bearing with quadratic and cubic terms and time-varying stiffness, *Nonlinear Dynamics*, 2005, **41**, 331-359, doi: 10.1007/s11071-005-7959-2.
[25] W. Zhang, M. H. Yao, X. P. Zhan, Multi-pulse chaotic motions of a rotor-active magnetic bearing system with time-varying stiffness, *Chaos, Solitons & Fractals*, 2006, **27**, 175-186, doi: 10.1016/j.chaos.2005.04.003.
[26] J. I. Inayat-Hussain, Chaos *via* torus breakdown in the vibration response of a rigid rotor supported by active magnetic bearings, *Chaos, Solitons & Fractals*, 2007, **31**, 912-927, doi: 10.1016/j.chaos.2005.10.039.
[27] A. Heydari, M. Mirparizi, F. Shakeriaski, F. S. Samani, M. Keshavarzi, Nonlinear vibration analysis of a rotor supported by magnetic bearings using Homotopy perturbation method, *Propulsion and Power Research*, 2017, **6**, 223-232, doi: 10.1016/j.jppr.2017.07.004.
[28] W. Zhang, R. Q. Wu, B. Siriguleng, Nonlinear vibrations of a rotor-active magnetic bearing system with 16-pole legs and two degrees of freedom, *Shock and Vibration*, 2020, **2020**, 5282904, doi: 10.1155/2020/5282904.
[29] N. A. Saeed, M. Eissa, W. A. El-Ganini, Nonlinear oscillations of rotor active magnetic bearings system, *Nonlinear Dynamics*, 2013, **74**, 1-20, doi: 10.1007/s11071-013-0967-8.
[30] H. M. Navazi, M. Hojjati, Nonlinear vibrations and stability analysis of a rotor on high-static-low-dynamic-stiffness supports using method of multiple scales, *Aerospace Science and Technology*, 2017, **63**, 259-265, doi: 10.1016/j.ast.2017.01.007.
[31] M. Rizwan Shad, G. Michon, A. Berlioz, Modeling and analysis of nonlinear rotordynamics due to higher order deformations in bending, *Applied Mathematical Modelling*, 2011, **35**, 2145-2159, doi: 10.1016/j.apm.2010.11.043.
[32] M. Eissa, M. Kamel, H. S. Bauomy, Nonlinear behavior of tuned rotor-amb system with time varying stiffness, *International Journal of Bifurcation and Chaos*, 2011, **21**, 195-207, doi: 10.1142/s0218127411028362.
[33] M. Kamel, H. S. Bauomy, Nonlinear behavior of a rotor-AMB system undermulti-parametric excitations, *Meccanica*, 2010, **45**, 7-22, doi: 10.1007/s11012-009-9213-3.
[34] A. D. Shaw, A. R. Champneys, M. I. Friswell, Normal form analysis of bouncing cycles in isotropic rotor stator contact problems, *International Journal of Mechanical Sciences*, 2019, **155**, 83-97, doi: 10.1016/j.ijmecsci.2019.02.035.
[35] J. C. Ji, Stability and Hopf bifurcation of a magnetic bearing system with time delays, *Journal of Sound and Vibration*, 2003, **259**, 845-856, doi: 10.1006/jsvi.2002.5125.
[36] A. Yektanezhad, S. A. A. Hosseini, H. Tourajizadeh, M. Zamanian, Vibration analysis of flexible shafts with active magnetic bearings, *Iranian Journal of Science and Technology, Transactions of Mechanical Engineering*, 2020, **44**, 403-414, doi: 10.1007/s40997-018-0263-9.
[37] A. Y. T. Leung, Z. Guo, Resonance response of a simply supported rotor-magnetic bearing system by harmonic balance, *International Journal of Bifurcation and Chaos*, 2012, **22**, 1250136, doi: 10.1142/s0218127412501362.
[38] H. Sasaki, S. Kamada, T. Sugiura, Subharmonic resonance due to gap between geometric and magnetic centers of rotor supported by superconducting magnetic bearing, *IEEE Transactions on Applied Superconductivity*, 2016, **26**, 5206505, doi: 10.1109/TASC.2016.2549039.
[39] N. A. Saeed, E. Mahrous, E. Abouel Nasr, J. Awrejcewicz, Nonlinear dynamics and motion bifurcations of the rotor active magnetic bearings system with a new control scheme and rub-impact force, *Symmetry*, 2021, **13**, 1502, doi: 10.3390/sym13081502.
[40] K. Li, C. Peng, Z. Deng, W. Huang, Z. Zhang, Field dynamic balancing for active magnetic bearings supporting rigid rotor shaft based on extended state observer, *Mechanical Systems and Signal Processing*, 2021, **158**, 107801, doi: 10.1016/j.ymssp.2021.107801.
[41] S. M. El-Shourbagy, N. A. Saeed, M. Kamel, K. R. Raslan,

M. K. Aboudaif, J. Awrejcewicz, Control performance, stability conditions, and bifurcation analysis of the twelve-pole active magnetic bearings system, *Applied Sciences*, 2021, **11**, 10839, doi: 10.3390/app112210839.
[42] R. Trentini, D. Dos Santos, O. H. Reichow, R. Piontkewicz, Dynamic modeling and parametric analysis of the magnetic stiffness on a radial heteropolar rotor magnetic bearing (RMB), *International Journal of Electrical and Computer Engineering Research*, 2021, **1**, 9-14, doi: 10.53375/ijecer.2021.18.
[43] P. Zhang, C. Zhu, Vibration control of base-excited rotors supported by active magnetic bearing using a model-based compensation method, *IEEE Transactions on Industrial Electronics*, 2024, **71**, 261-270, doi: 10.1109/TIE.2023.3243263.
[44] B. Xu, J. Zhou, L. Xu, Vibration suppression for a slice rotor supported by active magnetic bearings based on fractional-order adaptive backstepping control, *Mechanical Systems and Signal Processing*, 2024, **210**, 111160, doi: 10.1016/j.ymssp.2024.111160.
[45] A. Kandil, L. Hou, M. Sharaf, A. A. Arafa, Configuration angle effect on the control process of an oscillatory rotor in 8-pole active magnetic bearings, *AIMS Mathematics*, 2024, **9**, 12928-12963, doi: 10.3934/math.2024631.
[46] W. S. Ma, F. H. Liu, S. F. Lu, X. J. Song, S. Huang, Y. K. Zhu, X. Jiang, Nonlinear dynamics and motion bifurcations of 12-pole variable stiffness rotor active magnetic bearings system under complex resonance, *International Journal of Non-Linear Mechanics*, 2025, **169**, 104958, doi: 10.1016/j.ijnonlinmec.2024.104958.